Author Manuscript Published OnlineFirst on February 13, 2018; DOI: 10.1158/1535-7163.MCT-17-0634
Author manuscripts have been peer reviewed and accepted for publication but have not yet been edited.

AACR American Association for Cancer Research

Molecular Cancer Therapeutics

A Spatio-temporal Model of Macrophage-mediated Drug Resistance in Glioma Immunotherapy

Yongjiang Zheng, Jiguang Bao, Qiyi Zhao, et al.

Mol Cancer Ther Published OnlineFirst February 13, 2018.

Updated version	Access the most recent version of this article at: doi:10.1158/1535-7163.MCT-17-0634
Supplementary Material	Access the most recent supplemental material at: http://mct.aacrjournals.org/content/suppl/2018/02/13/1535-7163.MCT-17-0634.DC1
Author Manuscript	Author manuscripts have been peer reviewed and accepted for publication but have not yet been edited.

E-mail alerts	Sign up to receive free email-alerts related to this article or journal.
Reprints and Subscriptions	To order reprints of this article or to subscribe to the journal, contact the AACR Publications Department at pubs@aacr.org.
Permissions	To request permission to re-use all or part of this article, use this link http://mct.aacrjournals.org/content/early/2018/02/13/1535-7163.MCT-17-0634. Click on "Request Permissions" which will take you to the Copyright Clearance Center's (CCC) Rightslink site.

Downloaded from mct.aacrjournals.org on February 14, 2018. © 2018 American Association for Cancer Research.

Cancer Biology and Translational Studies

Molecular Cancer Therapeutics

A Spatio-Temporal Model of Macrophage-Mediated Drug Resistance in Glioma Immunotherapy

Yongjiang Zheng[1], Jiguang Bao[2], Qiyi Zhao[3], Tianshou Zhou[4], and Xiaoqiang Sun[5,6]

Abstract

The emergence of drug resistance is often an inevitable obstacle that limits the long-term effectiveness of clinical cancer chemotherapeutics. Although various forms of cancer cell-intrinsic mechanisms of drug resistance have been experimentally revealed, the role and the underlying mechanism of tumor microenvironment in driving the development of acquired drug resistance remain elusive, which significantly impedes effective clinical cancer treatment. Recent experimental studies have revealed a macrophage-mediated drug resistance mechanism in which the tumor microenvironment undergoes adaptation in response to macrophage-targeted colony-stimulating factor-1 receptor (CSF1R) inhibition therapy in gliomas. In this study, we developed a spatio-temporal model to quantitatively describe the interplay between glioma cells and CSF1R inhibitor-targeted macrophages through CSF1 and IGF1 pathways. Our model was used to investigate the evolutionary kinetics of the tumor regrowth and the associated dynamic adaptation of the tumor microenvironment in response to the CSF1R inhibitor treatment. The simulation result obtained using this model was in agreement with the experimental data. The sensitivity analysis revealed the key parameters involved in the model, and their potential impacts on the model behavior were examined. Moreover, we demonstrated that the drug resistance is dose-dependent. In addition, we quantitatively evaluated the effects of combined CSFR inhibition and IGF1 receptor (IGF1R) inhibition with the goal of designing more effective therapies for gliomas. Our study provides quantitative and mechanistic insights into the microenvironmental adaptation mechanisms that operate during macrophage-targeted immunotherapy and has implications for drug dose optimization and the design of more effective combination therapies. *Mol Cancer Ther; 1–13. ©2018 AACR.*

Introduction

As a microenvironment-targeted immunotherapy, colony-stimulating factor-1 receptor (CSF1R) inhibition is expected to be a promising therapeutic strategy for high-grade gliomas (1, 2). Although multiple clinical trials testing the efficacy of CSF1R inhibition have been conducted in glioma patients, it is unclear whether and how resistance emerges during this therapy. Recently, a preclinical study using a genetic mouse model (3) showed that a high percentage (>50%) of glioblastoma multiformes (GBM) recur in the mice following treatment via long-term CSF1R inhibition, although overall survival is significantly prolonged. Therefore, it is important and timely to investigate the mechanisms underlying the acquisition of resistance to CSF1R inhibition and quantitatively determine the key biological parameters involved in this process.

Many types of tumor cell-intrinsic mechanisms, including genetic mutations and epigenetic modifications (4), signaling network rewiring (5–7), cellular heterogeneity involving cancer stem cells (8, 9), and drug metabolism and pharmacodynamics (10), have been studied widely. Distinct from the above mechanisms, the roles of tumor microenvironment in driving and facilitating tumor growth and drug resistance have been revealed and acknowledged with increasing attention in recent years (3, 11–13). Actually, the tumor microenvironment involves multiple cell types, such as fibroblasts, endothelial cells and immune cells, that can interact with tumor cells (14). For example, immune cells, including macrophages, dendritic cells, neutrophils, Treg cells, T effector cells, natural killer cells, etc. (15), can interact with tumor cells either via direct cell–cell contacts or via soluble factors such as secreted cytokines or growth factors (16). Such cross-talk between immune and tumor cells plays substantial roles before and during tumor growth as well as the in the development of drug resistance (17).

To investigate the dynamic interactions between cancer cells and the associated microenvironment in the context of therapeutic intervention, the traditional experimental approach requires multiple experimental conditions and time points and, thus, is time consuming and expensive. Therefore, a computational systems biology approach is necessary to address this issue. Mathematical modeling is a powerful tool for the quantitative investigation of dynamic biological systems that can provide insights

[1]Department of Hematology, The Third Affiliated Hospital of Sun Yat-Sen University, Guangzhou, China. [2]School of Mathematical Sciences, Beijing Normal University, Beijing, China. [3]Department of Infectious Diseases, The Third Affiliated Hospital of Sun Yat-Sen University, Guangzhou, China. [4]School of Mathematical and Computational Science, Sun Yat-Sen University, Guangzhou, China. [5]Zhong-shan School of Medicine, Sun Yat-Sen University, Guangzhou, China. [6]Key Laboratory of Tropical Disease Control (Sun Yat-Sen University), Chinese Ministry of Education, Guangzhou, Guangdong, China.

Note: Supplementary data for this article are available at Molecular Cancer Therapeutics Online (http://mct.aacrjournals.org/).

Corresponding Author: Xiaoqiang Sun, Sun Yat-Sen University, Guangzhou 510080, China. Phone: 86-136-3244-0342; E-mail: sunxq6@mail.sysu.edu.cn; xiaoqiangsun88@gmail.com

doi: 10.1158/1535-7163.MCT-17-0634

©2018 American Association for Cancer Research.

into underlying mechanisms and experimentally testable predictions. From a quantitative biology perspective, we can ask questions regarding the effects of dose on drug resistance and the influence of critical parameters on the evolution of drug resistance. Driven by the hypothesis that an appropriately simplified mathematical model is able to capture the key kinetics of microenvironment-mediated drug resistance, we seek to mechanistically model the spatio-temporal evolution of interactions within the tumor-microenvironment system during drug treatment.

In the past decade, several theoretical models have been developed to investigate the role of the microenvironment in tumor growth [e.g., refs. (18–21)]. Moreover, some efforts using modeling approaches to investigate the role of the microenvironment in drug resistance have also been conducted recently. For instance, Lindsay and colleagues (22) developed a stochastic model to simulate the effect of oxygen on the growth kinetics of cancer cells and to investigate the potential benefits of combining hypoxia-activated prodrugs with standard targeted therapy to prevent drug resistance in non–small cell lung cancer. In addition, our previous study (23) designed a modeling framework using stochastic differential equations to simulate the therapy-induced microenvironmental adaptation that promotes the growth and metastasis of resistant tumor cells, and therefore contributes to the development of the acquired drug resistance. However, no modeling work has been dedicated to investigating the kinetics of drug resistance driven by the immune microenvironment, particularly involving macrophages, in cancer therapy.

Recently, the experimental studies have revealed a macrophage-mediated drug resistance mechanism in glioma immunotherapy (3). Specifically, in the absence of CSF1R inhibition, tumor-associated macrophages exhibit a protumorigenic M2 phenotype and contribute to glioma progression. However, when targeted by CSF1R inhibitors, macrophages switch to an antitumorigenic M1 phenotype with enhanced phagocytosis, thereby promoting tumor cell death. Following prolonged treatment with CSF1R inhibitors, accumulated IL4 from other cell types (e.g., T cells) stimulates macrophages to secrete insulin-like growth factor 1 (IGF1) into the microenvironment, which in turn sustains the survival and growth of glioma cells (3).

On the other hand, certain mathematical models have also recently been developed to describe the interactions between cancer cells and macrophages during cancer progression. For example, Szomolay and colleagues (24) proposed a system of partial differential equations (PDE) to simulate the macrophages-mediated interactions among tumor cells and endothelial cells through several cytokines, including M-CSF1, GM-CSF1, VEGF, and MCP-1, as well as oxygen. Their model simulations are consistent with the *in vivo* data obtained under different conditions of GM-CSF (granulocyte/macrophage colony-stimulating factor) exposure, allowing the model to predict treatment outcomes. Knútsdóttir and colleagues (25) described paracrine and autocrine signaling (i.e., CSF1/CSF1R and EGF/EGFR pathways) between tumor cells and macrophages using both PDEs model and cell-based discrete 3D simulation. The authors identified parameters responsible for the observed ratio of tumor cell to macrophage and demonstrated how CSF1/CSF1R autocrine signaling in tumor cells affect this ratio. These works provided the modeling basis and implicated potential values of theoretically investigating the interactions between tumor cells and macrophages.

In this study, based on the above experimentally validated mechanism (3), we developed a spatio-temporal model to quantitatively describe the interplay between glioma cells and CSF1R inhibition-induced transition of macrophage M2 and M1 phenotypes through dynamic CSF1/CSF1R and IGF1/IGF1R pathways. Our mode was used to investigate the response of glioma cells to macrophage-targeted CSF1R inhibition therapy and the associated dynamic adaptation of the tumor microenvironment. The simulation result obtained using this model is in agreement with the experimentally observed regrowth phenomenon of resistant gliomas and quantitative survival times (3). Moreover, we demonstrated that the drug resistance is dose-dependent. In addition, we quantitatively evaluated the effects of combined CSFR inhibition and IGF1 receptor (IGF1R) inhibition with the goal of designing more effective therapies for gliomas.

Materials and Methods

PDE model

We model the spatio-temporal evolution of cancer cells and their microenvironment during CSF1R inhibition based on the experimentally validated mechanism (ref. 3; Fig. 1). The major assumptions of our model include:

a) The numbers of cancer cells and macrophages as well as levels of secreted soluble factors including CSF1, IGF1, and IL4 are large enough such that they can be treated as continuous variables. So, the numbers of cells and levels of cytokines are described by their densities and concentrations, respectively.
b) Glioma cells, macrophages, CSF1, IGF1, and drugs are subject to diffusion; glioma cells and macrophages are also subject to chemotaxis in response to IGF1 and CSF1, respectively.
c) The proliferation rate and the death rate of tumor cells are regulated by IGF1 and CSF1R inhibitor. Specifically, by regulating the phenotype transition between M1 and M2 macrophages, CSF1R inhibition does not only increase apoptosis rate of glioma cells but also decreases their proliferation

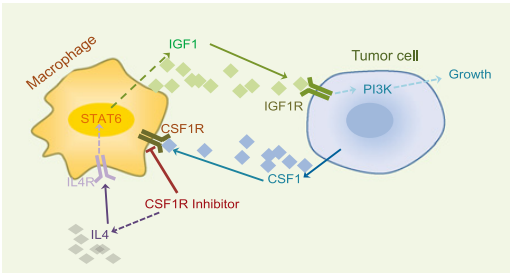

Figure 1.
Schematic representation of how adaptation of the tumor microenvironment contributes to acquired drug resistance during CSF1R inhibition therapy of gliomas (3). Macrophages and glioma cells can interact through the CSF1/CSF1R and IGF1/IGF1R pathways. CSF1R, a critical receptor on macrophages, is a promising immunotherapeutic target in gliomas and is undergoing clinical evaluation. In the absence of CSF1R inhibition, macrophages exhibit a protumorigenic M2 phenotype that promotes glioma progression. When targeted by a CSF1R inhibitor, macrophages switch to an antitumorigenic phenotype that promotes tumor cell death. On the other hand, following prolonged treatment, elevated macrophage-derived IGF1, which is promoted by IL4 secreted by other cell types (e.g., T cells), in turn sustains the survival and growth of glioma cells.

rate (26). Meanwhile, the CSF1R inhibitor-induced IGF1 secretion from macrophages through IL4 signaling could, in turn, sustains the proliferation of glioma cells (3).

d) The CSF1R inhibitor treatment does not significantly affect the number of tumor-associated macrophages, as experimental studies indicated (27). As such, the total density of tumor-associated macrophages is assumed to be constant during CSF1R inhibition treatment.

We used a set of PDEs to model the growth, death, and migration of cancer cells and tumor-associated macrophages and the diffusion/secretion/degradation of CSF1, IGF1, and drugs. The time scale of this entire mechanism is about 200 days in accordance with the experimental study (3).

The migration of glioma cells consists of random diffusion and chemotaxis toward the chemical gradients of signals. We assumed a logistic growth rate and a linear death rate of cancer cells (28, 29). Therefore, the equation that describes the evolution of the tumor cell density (C_T) is as follows:

$$\frac{\partial C_T}{\partial t} = D_T \Delta C_T - a_T \nabla \cdot (C_T \nabla [IGF1]) + \tilde{r}_T C_T \left(1 - \frac{C_T}{C_T^{\max}}\right) - \tilde{d}_T C_T, \quad (1)$$

where D_T is the diffusion coefficient of glioma cells and a_1 is the chemotaxis coefficient for glioma cells with respect to IGF1. $C_T^{\max}$ represents the maximal carrying capacity of the cancer cells. $\tilde{r}_T$ and $\tilde{d}_T$ are the proliferation rate and the death rate, respectively, which are regulated by the IGF1 and CSF1R inhibitor. Experimental data (3, 26) have revealed that CSF1R inhibition does not only increase apoptosis of glioma cells but also decreases their proliferation. Although the CSF1R inhibitor-induced IGF1 secretion from macrophages could promote the proliferation of glioma cells (3). Therefore, the regulated proliferation rate of glioma cells is modeled by the following equation:

$$\tilde{r}_T = r_T \cdot H_1(IGF1) \cdot \left(\alpha \cdot C_\phi \cdot H_2(CSF1R_I)\right), \quad (2)$$

where r_T is the basic proliferation rate of tumor cells and α is a regulatory coefficient for the macrophage density (C_ϕ) corresponding to M2 macrophages' protumorigenic function. Hill functions (30–32) for the activation and repression processes were used to describe the roles of IGF1 and CSF1R inhibitors ($CSF1R_I$) in regulating the proliferation rate of glioma cells as follows:

$$H_1(IGF1) = \frac{[IGF1]}{K_1 + [IGF1]},$$

$$H_2(CSF1R_I) = \frac{1}{1 + [CSF1R_I]/K_2},$$

where K_1 and K_2 are Michaelis–Menten constants.

The apoptosis of glioma cells is accelerated by treatment with a CSF1R inhibitor (3, 26), as described above; therefore, the regulated death rate of glioma cells is described by the following equation:

$$\tilde{d}_T = d_T \cdot \left(1 + \beta \cdot C_\phi \cdot H_3(CSF1R_I)\right), \quad (3)$$

where d_T is the basic death rate of glioma cells and β is a regulatory coefficient corresponding to M1 macrophages' antitumorigenic function. The pro-apoptotic role of the CSF1R inhibitor was modeled as

$$H_3(CSF1R_I) = \frac{[CSF1R_I]}{K_3 + [CSF1R_I]},$$

where K_3 is a Michaelis–Menten constant.

Tumor-associated macrophages are recruited to tumor sites by chemoattractants such as CSF1 (33, 34); this process can be modeled by the following equation:

$$\frac{\partial C_\phi}{\partial t} = D_\phi \Delta C_\phi - a_\phi \nabla \cdot \left(C_\phi \nabla [CSF1]\right), \quad (4)$$

where D_ϕ is the diffusion coefficient of the random walk of macrophages and a_ϕ is the chemotaxis coefficient of CSF1. The experimental studies have demonstrated that CSF1R inhibition did not affect the number of tumor-associated macrophages (26, 27). Therefore, the total macrophage density is assumed to be constant, as also reported in refs. (25, 35). Therefore, the net growth and death rates of macrophages are zero in the above equation. The above Eq. (4) is a simplification of the tumor-associated macrophage population which involves both M1 and M2-type macrophages. M1 macrophages exhibit antitumorigenic phenotype with enhanced phagocytosis, whereas M2 macrophages are protumorigenic and contribute to glioma growth and progression. However, CSF1R inhibition alters macrophages' phenotypes switched from M2 to M1 (27). Functions of these two phenotypes are modeled in Eqs. (2, 3), respectively. The CSF1R inhibitor induced phenotype switch of macrophages from M2 to M1 is reflected by the decrease of protumor function of M2 macrophages ($\alpha \cdot C_\phi$) through repression Hill function $H_2(CSF1R_I)$ and the increase of antitumor function of M1 macrophage ($\beta \cdot C_\phi$) through activation Hill function $H_3(CSF1R_I)$. Furthermore, because populations of both these two types of macrophage are subject to diffusion and chemotaxis as in Eq. (4), for simplicity we do not describe the two types separately.

CSF1 is overexpressed in human glioblastomas (36) and can be synthesized and produced in both cell-surface form and secreted form (37). The secreted CSF1 by glioma cells then diffuses into the microenvironment. Therefore, the concentration of CSF1 is modeled by the following equation:

$$\frac{\partial [CSF1]}{\partial t} = D_{CSF1} \Delta [CSF1] + S_{CSF1} \cdot C_T - d_{CSF1} \cdot [CSF1], \quad (5)$$

where D_{CSF1} represents the diffusion rate of CSF1. S_{CSF1} and d_{CSF1} are the rate of CSF1 secretion by tumor cells and the CSF1 degradation rate, respectively.

IGF1 secretion from macrophages is promoted by IL4 signaling. We model the evolution of the IGF1 concentration as follows:

$$\frac{\partial [IGF1]}{\partial t} = D_{IGF1} \Delta [IGF1] + S_{IGF1} \cdot C_\phi \cdot [IL4] - d_{IGF1} \cdot [IGF1], \quad (6)$$

where D_{IGF1}, S_{IGF1} and d_{IGF1} are the diffusion, secretion and degradation rates of IGF1, respectively. Following treatment with a CSF1R inhibitor, IL4 is secreted from multiple cell types, including T cells and its concentration is elevated. The experimental data (3) indicate that the numbers of many types of

immune cells (e.g., neutrophils, monocytes, dendritic-like cells, B cells, helper T cells and regulatory T cells) in drug-resistant group of mice are not significantly different from that in control group. As such, we do not explicitly describe the densities of IL4-secreting cells in the model for simplicity. We assume that the rate of change in the concentration of IL4 is proportional to the concentration of the CSF1R inhibitor with a coefficient of S_{IL4}; that is, the secretion of IL4 can be modeled by the following equation:

$$\frac{\partial[IL4]}{\partial t} = S_{IL4} \cdot [CSF1R_I]. \tag{7}$$

Solving this equation and substituting it into Eq. (6) yields the following equation:

$$\begin{aligned}\frac{\partial[IGF1]}{\partial t} &= D_{IGF1}\Delta[IGF1] \\ &+ S_{IGF1} \cdot C_{\phi} \cdot [IL4]_0 \cdot \left(1 + S_{IL4} \cdot \int_0^t [CSF1R_I](s)ds\right) \\ &- d_{IGF1} \cdot [IGF1],\end{aligned} \tag{8}$$

where $[IL4]_0$ is the initial concentration of IL4 in the absence of treatment with the CSF1R inhibitor.

In addition, we model the diffusion and degradation of drugs (including CSF1R inhibitors and IGF1R inhibitors) as follows:

$$\frac{\partial[Drug]}{\partial t} = D_{drug}\Delta[Drug] - \eta_{drug}, \tag{9}$$

where D_{drug} is the diffusion rate of the drug and η_{drug} is the degradation rate or the uptake rate of the drug by cells.

Non-dimensionization and radial symmetry simplification

To reduce the number of parameters, we simplify the PDE model by rescaling the equations into a dimensionless form (Supplementary Text S1). Furthermore, for simplicity, we assumed a spherical model for the tumor and its microenvironment. Therefore, the domain we consider is a spheroid. Assuming radial symmetry, the cell density and cytokine concentration evolve in the domain [0, L]. The details of radial symmetry simplification are provided in Supplementary Text S2.

Initial and boundary conditions

The initial and boundary conditions are given in Supplementary Text S3. In particularly, the addition of the drug is modeled with a Dirichlet boundary condition $[Drug]|_L = d_{\max}$.

Numerical simulation

We solve the system of the dimensionless PDEs (Eqs. Supplementary S11–S15) numerically using the *pdepe* solver in MATLAB R2007b (MathWorks), which automatically and dynamically selects time steps and is capable of solving PDEs with multiple temporal orders (38). The length of the simulation domain (L) is approximately 4 cm. The numerical simulation results are evaluated at locations with spatial step of 0.08 cm and time points with step of 1 day.

Parameter sensitivity analysis

Most parameters in the model are obtained from experimental measurements, whereas some others are estimated or calibrated. The details of parameter estimation were described in Supplementary Text S4. Supplementary Tables S1 and S2 list the original parameters and the dimensionless parameters, respectively, used in the simulation. To examine whether the parameter variations significantly affect the model output of interest, we implement sensitivity analyses of the most relevant parameters, i.e., A_T, A_ϕ, r_T, d_T, B_1, B_2, e, D_d, and η_d.

A sampling-based global sensitivity analysis (39) is performed. For each parameter, we use Latin hypercube sampling to generate 1,000 samples in the range of $[1/5p_0, 5p_0]$, where p_0 is the baseline value of the parameter. All parameters are varied simultaneously for the simulations.

For the varied parameters, we choose the killing rate and the regrowth rate of cancer cells as model outputs to evaluate the long-term effects of parameter variations on the drug response and resistance. The killing rate of cancer cells is defined as

$$R_K = \frac{\bar{C}_T(0) - \bar{C}_T(t_1)}{t_1}, \tag{10}$$

where $\bar{C}_T$ represents the average cancer cell density and t_1 is the time at which the minimal average cancer cell density is achieved. Similarly, the regrowth rate of cancer cell density is defined as

$$R_G = \frac{\bar{C}_T(t_2) - \bar{C}_T(t_1)}{t_2 - t_1}, \tag{11}$$

where t_2 is the length of time over which the simulation performed.

For each parameter, the partial correlation coefficient between the simulated model output (R_K or R_G) and the sampled parameter values is calculated and is defined as a global sensitivity coefficient in this study.

A local parameter sensitivity analysis (Supplementary Text S5) is also performed to investigate the dose-dependent sensitivities of parameters and to assess the combinatorial effects of the parameters on drug resistance.

Results

The evolution profiles of the tumor and microenvironment in response to CSF1R inhibitor treatment

We used our mathematical model to investigate the evolution profile of the tumor and the associated microenvironment under the condition of treatment with a CSF1R inhibitor. The drug response of a high-grade glioma tumor (with a radius of approximately 4 cm) to treatment with a CSF1R inhibitor (3 doses) was simulated (Fig. 2). As shown in Fig. 2A, at the early stage, the cancer cell density decreased dramatically after a dozen days. However, the tumor regrew after a long-term dormancy period of approximately 150 days. At day 200, the cancer cell density was restored to nearly the level that was comparable before the treatment. The changes in macrophage density and the concentrations of CSF1 and IGF1 in the tumor microenvironment during the CSF1R inhibitor treatment were also examined (Fig. 2B–D). As expected, the change in the CSF1 concentration exhibited similar pattern with the evolution of the cancer cell density, whereas the IGF1 concentration kept increasing over

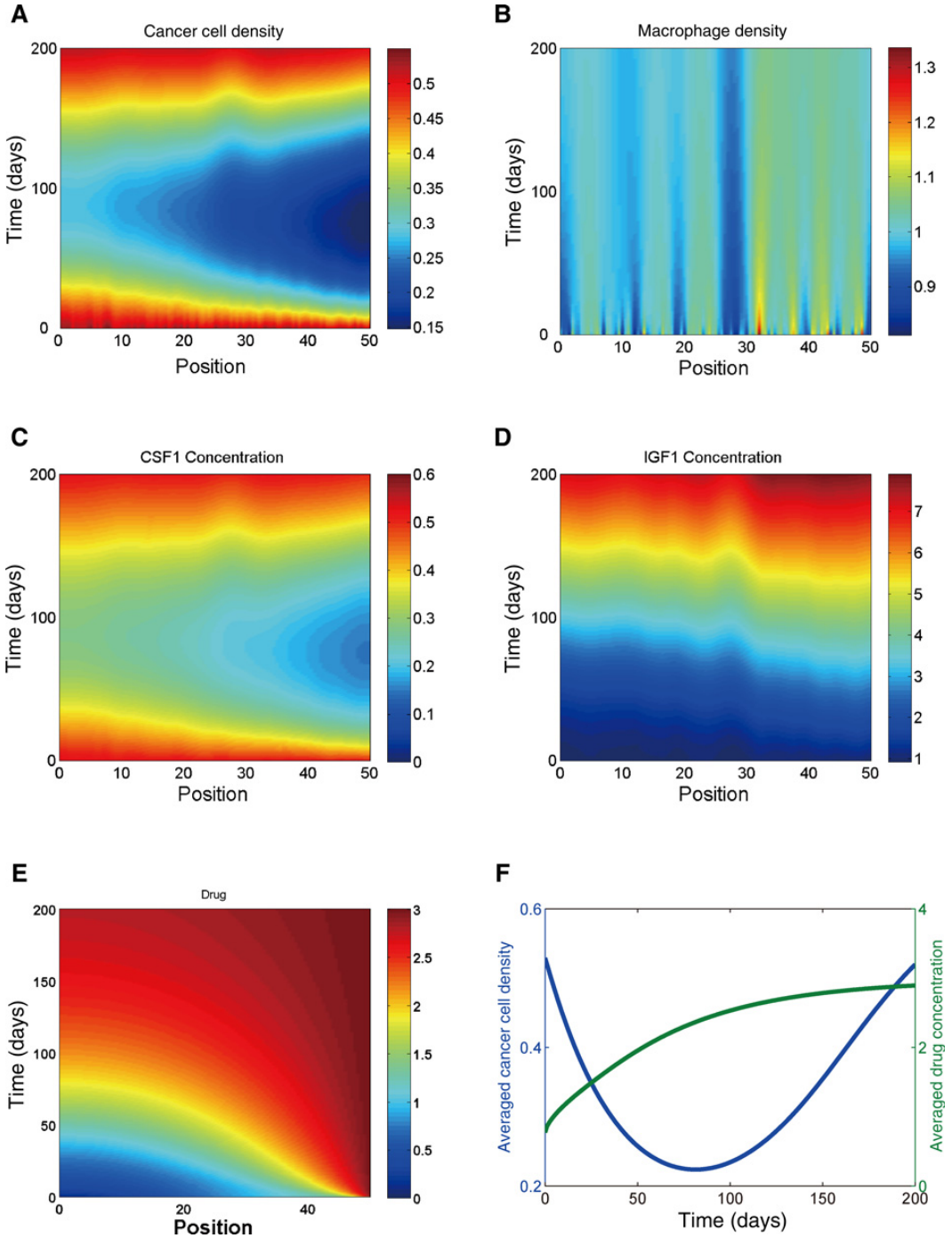

Figure 2.

Drug response of cancer cells and adaptation of the tumor microenvironment in the context of therapeutic intervention with CSF1R inhibition. The spatio-temporal distributions of (**A**) cancer cell density, (**B**) macrophage density, (**C**) CSF1 concentration, (**D**) IGF1 concentration, and (**E**) drug concentration. **F,** Curves of time course of average cancer cell density and average drug concentration.

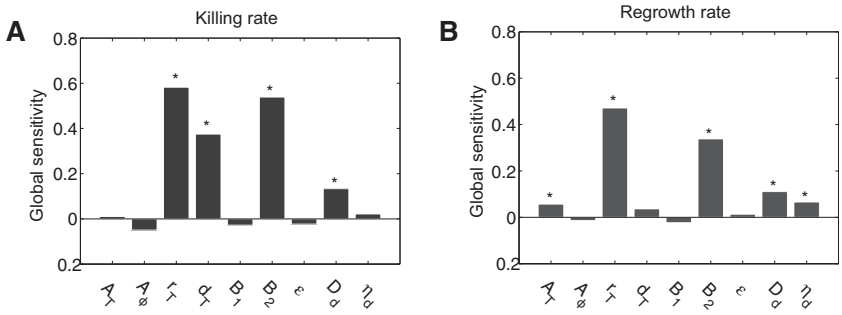

Figure 3.
Parameter sensitivity analysis. **A,** Global sensitivity analyses of the cancer cell killing rate with respect to the model parameters. **B,** Global sensitivity analyses of the cancer cell regrowth rate with respect to the model parameters. Positive sensitivity indicates that increasing the corresponding parameter leads to an increase in the killing rate or the regrowth rate. (*) indicates that the sensitivity for the corresponding parameter is significantly ($P < 0.05$) different from zero. The drug dose was 3 in the simulation.

time. Figure 2E shows the evolution profile of the concentration of CSF1R inhibitor. In addition, Fig. 2F shows the time courses of average cancer cell density and average drug concentration. Our model observed similar regrowth of resistant gliomas under the treatment of CSF1R inhibitor as previously reported (Fig. 1B in ref. 3).

Key parameters affecting the dynamics of drug resistance

To determine which parameters are more sensitive and critical for the killing rate and the regrowth rate of cancer cells during treatment with a CSF1R inhibitor, we performed a global parameter sensitivity analysis (see Supplementary Text S3). Figure 3 shows the results of the global sensitivity analysis. The killing rate (Fig. 3A) and the regrowth rate (Fig. 3B) display different sensitivities with respect to variations in the parameters. The significant sensitive parameters for the killing rate are r_T, d_T, B_2, and D_d, whereas the significant sensitive parameters for the regrowth rate are A_T, r_T, B_2, D_d, and η_d.

To confirm that the emergence of the regrowth of the cancer cells is not caused by the decreased drug concentration due to drug degradation or consumption, we examined the spatio-temporal profiles of cancer cells and their microenvironment using the model with increased drug consumption rate (10-fold of η_{drug}; Supplementary Fig. S1). The simulation results showed that increasing the drug consumption rate did not significantly influence the emergence of drug resistance, compared with Fig. 2.

We also examined the behavior of the model using different values of certain important parameters, including r_T, d_T, B_2, and D_d (Supplementary Fig. S2). A decrease in the value of r_T (growth rate of tumor cells) and an increase in d_T (death rate of tumor cells), as well as a decrease in B_2 (secretion rate of IGF1), resulted in the disappearance of the emergence of drug resistance. In addition, the diffusion rate of the drug (D_d) also affected the killing and regrowth rates of the resistant cancer cells.

Stochasticity in the secretion rate of IGF1 results in heterogeneous drug resistance

The secretion rate of IGF1 (B_2) is a critical parameter for the macrophage-mediated drug resistance as described above (Fig. 3). Therefore, we then examined whether stochasticity in IGF1 secretion rate could result in heterogeneous drug resistance. We assumed a bimodal distribution of B_2 and used the Monte Carlo method to simulate the stochastic temporal evolution of cancer cell density in a population of N glioma patients. The details of the stochastic simulation and the computation of the distribution of survival times were described in Supplementary Text S6.

Figure 4A shows the heterogeneous evolution of cancer cell density in different patients in response to drug treatment. Each curve represents one patient. The simulation demonstrated that the cancer cell density was reduced in some patients but some tumors regrew. Furthermore, Fig. 4B shows the theoretical survival curves, representing the changes of survival percentages over time, of the glioma patients with and without CSF1R inhibition treatment (red line and gray line, respectively). The predicted significant difference between these two curves and their trends are in good agreement with the preclinical data (Fig. 1D in ref. 3). Moreover, we quantified the survival percentage, $SP(t_i)$, from the experimental data (Fig. 1D in ref. 3) and calculated the corresponding survival frequency according to $f(t_i) = SP(t_i) - SP(t_{i+1})$, with results shown in Fig. 4C and D. The comparison between the simulated survival frequency and experimental data shows a good agreement between them.

Dose-dependent drug resistance

We further investigated the effect of dose on the drug response and resistance. Figure 5A displays curves for the time course of cancer cell density under conditions of treatment with different doses (0, 0.1, 0.5, 1, 2, and 3) of a CSF1R inhibitor. A low dose (e.g., less than 0.1) had a slight inhibitory effect on tumor growth. High doses killed cancer cells at the early stage but did not prevent tumor recurrence at a later stage. As the dose was increased, the rate of cancer cell death increased; however, the regrowth rate also increased due to drug resistance. A more comprehensive illustration of the "dose-temporal drug response" (Fig. 5B) demonstrated that different drug doses resulted in differential temporal evolutions of cancer cell density. The emergence of drug resistance, as well as its extent, depended on the dose of CSF1R inhibitor used.

Quantitative evaluation of the effect of combination drug therapy

To determine how the combined parameters affect the killing and regrowth rates of cancer cells during drug treatment, we performed a 2-parameter sensitivity analysis (see Supplementary Text S5). The results revealed that variations in the parameter combinations r_1&d_1, r_1&B_2, d_1&B_2, and d_1&B_2 influenced the killing rate of cancer cells more than other combinations

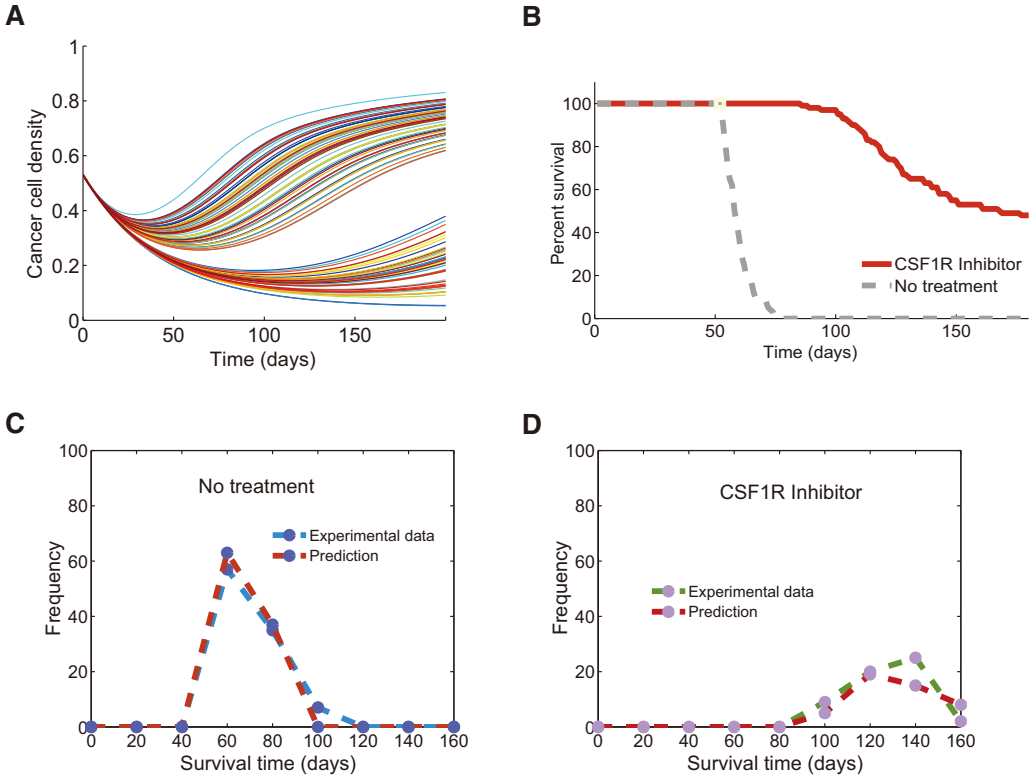

Figure 4.

Stochastic simulation and model validation with survival times. **A,** Stochastic time course of cancer cell density. Each curve represents one patient. **B,** Survival curves of patients treated with CSF1R inhibitor (solid red curve) or with no treatment (dashed gray curve). The significant difference between these two survival curves and their tendencies are in good agreement with existing preclinical data (3). **C,** Comparison between experimental data and prediction of the frequencies of survival times under no treatment condition. **D,** Comparison between experimental data and prediction of the frequencies of survival times under CSF1R inhibitor treatment condition.

(Supplementary Fig. S3A). For the regrowth rate, the most sensitive parameter combination was $r_1\&B_2$ (Supplementary Fig. S3B). These results indicate that combination therapy using drugs that both prevent cancer cell growth and inhibit the IGF1 signaling axis might be more effective than single CSF1R inhibition therapy.

Therefore, we evaluated the results of combination therapy using a CSF1R inhibitor and an IGF1R inhibitor (Fig. 6). The effect of IGF1R inhibition was incorporated into the model using the following equation:

$$\hat{R} = \tilde{R} \cdot \frac{1}{1 + [IGF1R_I]/K_1}, \quad (12)$$

where K_1 is a half-constant that was used to normalize the drug concentration of the IGF1R inhibitor. Therefore, K_1 was set to 1 in the simulation.

To quantitatively evaluate the synergy of the CSF1R-I and IGF1R-I co-treatment, a combination index based on Bliss independence (40, 41) was defined as follows:

$$CI(x_1, x_2) = E_{12}(x_1, x_2) - [E_1(x_1) + E_2(x_2) - E_1(x_1) \cdot E_2(x_2)], \quad (13)$$

where $E_i(x_i) = R_K(x_i) - R_G(x_i)$ quantifies the drug efficacy of the single CSF1R inhibitor ($i = 1$) or IGF1R inhibitor ($i = 2$) alone at dose x_i, $E_1(x_1) + E_2(x_2) - E_1(x_1)E_2(x_2)$ in Eq. (13) is the expected efficacy of the combination drug, and $E_{12}(x_1, x_2)$ is the actual outcome produced by the combination. Hence, the combination of CSF1R-I with IGF1R-I is synergistic if $CI > 0$, antagonistic if $CI < 0$, and additive if $CI = 0$.

Figure 6 demonstrates the dose-dependent effects of a combination therapy using a CSF1R inhibitor and an IGF1R inhibitor simultaneously. Figure 6A shows the time course of cancer cell density under conditions of treatment with single or combined CSF1R and IGF1R inhibitors. The combined intervention significantly reduced the resistance of the glioma to CSF1R inhibition. This prediction is consistent with experimental results (figure 7 in ref. (3) that the combination of BLZ945 (CSF1R inhibitor) and OSI906 (IGF1R inhibitor) significantly improved outcome in preclinical models. Figure 6B and C further shows the dependence of the killing and regrowth rates of the cancer cells on the drug dose. The regrowth rate decreased as the dose of IGF1R inhibitor was increased. In particular, at a dose of (1, 1), the killing rate was high, and the

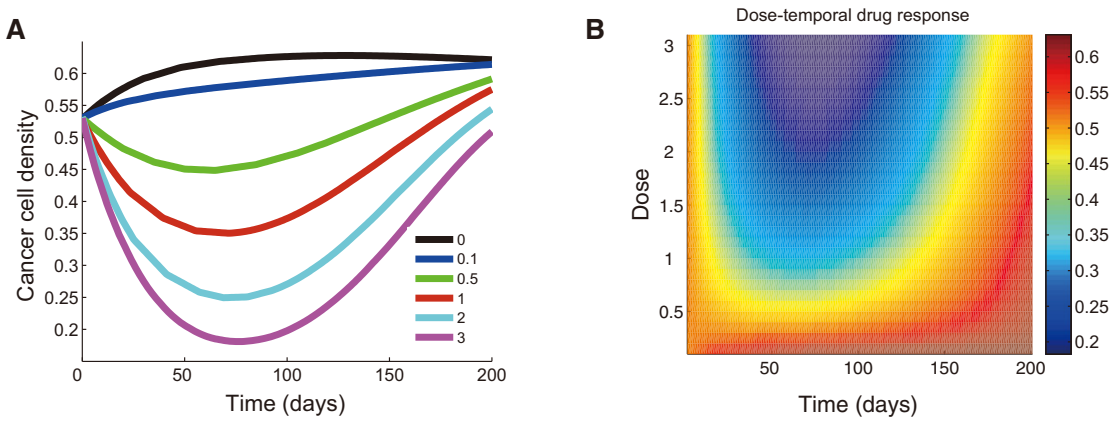

Figure 5.

Dose-dependent drug resistance. **A,** Time courses of the average cancer cell density under conditions of treatment with various doses (0, 0.1, 0.5, 1, 2, and 3) of a CSF1R inhibitor. **B,** Dose-temporal drug response of cancer cell density. Average density of cancer cells in the whole domain was shown.

regrowth rate was significantly decreased. Moreover, at these doses, the combination of a CSF1R inhibitor and an IGF1R inhibitor had a synergistic effect, as indicated by a positive combination index (Fig. 6D). Furthermore, the combination of CSF1R inhibition and IGF1R inhibition exhibited a pattern of dose-dependent synergy in which increasing doses resulted in less synergy, indicating the importance of drug dosages optimization.

Discussion

The tumor microenvironment plays multiple indispensable roles in cancer progression, and as such, targeting the tumor microenvironment has been proposed as a promising strategy for treating cancers (1, 2). Macrophages are of the most abundant immune cell types in the tumor microenvironment, the accumulation of which has been associated with the progression and high grade of various tumors, including gliomas (42, 43). Preclinical experiments using genetic mouse models have been conducted to demonstrate that macrophages can be targeted by inhibiting CSF1R to regress high-grade gliomas (3). However, like other targeted therapies, acquired resistance to CSF1R inhibition also occurs following long-term treatment (3).

In this study, we developed a simplified spatio-temporal model to mechanistically describe the response of glioma cells to CSF1R inhibition and the associated dynamic adaptation of the tumor microenvironment. The model simulations of tumor evolution and drug resistance are consistent with experimental results (3). The modeling framework provides a basis for the further investigation of tumor microenvironment-mediated drug resistance, provided that patient-specific data are available in future studies. Moreover, our results revealed a dose-dependent mechanism of resistance to CSF1R inhibition. Higher doses induced a greater regrowth rate of cancer cells compared with lower doses, although the killing rate was also increased. These results imply that multiple doses should be considered in experimental designs and/or clinical trials aiming to investigate resistance mechanisms and optimize drug doses.

The global parameter sensitivity analysis varies all the parameter simultaneously and evaluates the correlation between the overall model outputs and a set of sampled parameter values. Although the local parameter sensitivity analysis evaluates the local effect of the variation of a single parameter on the model output. The local parameter sensitivity analysis could differentiate the effect of different treatment conditions. A dose-dependent parameter sensitivity was revealed by the local sensitivity analysis (Supplementary Fig. S4) when treatment with different doses of CSF1R inhibitor was modeled. At a CSF1R inhibitor dose of 1 (Supplementary Fig. S4A and S4B), the most important parameters for the killing rate were the growth rate (r_1) and the death rate (d_1) of the cancer cells; other parameters were much less sensitive (Supplementary Fig. S4A). As the dose was increased to 3 (Supplementary Fig. S4C and S4D), the sensitivity coefficients of the parameters decreased except for that of parameter B_2, which influences the drug-induced secretion rate of IGF1 (Eq. Supplementary S14) in Supplementary Text S2). An important and interesting finding is that the relative sensitivity of the regrowth rate to the parameters r_1 and d_1 was altered as the drug dose increased from 1 to 3 (Supplementary Fig. S4B and S4D). Moreover, the regrowth rate was found to be more sensitive than the killing rate of cancer cells to parameter B_2.

We further investigated the impact of the initial spatial distribution of macrophages on the dynamics of drug response using different initial conditions of macrophages (Supplementary Text S3). The simulation results (Supplementary Figs. S5 and S6) demonstrated that, although the total densities of macrophages in these situations were set the same, the resistance kinetics of cancer cell density and spatio-temporal distribution profiles of cells and the secreted CSF1/IGF1 were different from that in Fig. 2. In particular, the simulation suggested that the higher ratio of macrophages close to the center of the tumor region, the higher density of resistant tumor cells on 200 days. These results illustrated the importance of the spatial distribution of tumor associated macrophages in mediating the resistance of CSF1R inhibition in gliomas.

We quantitatively evaluated the effects of combination therapy using CSF1R inhibition and IGF1R inhibition. Notably, we found

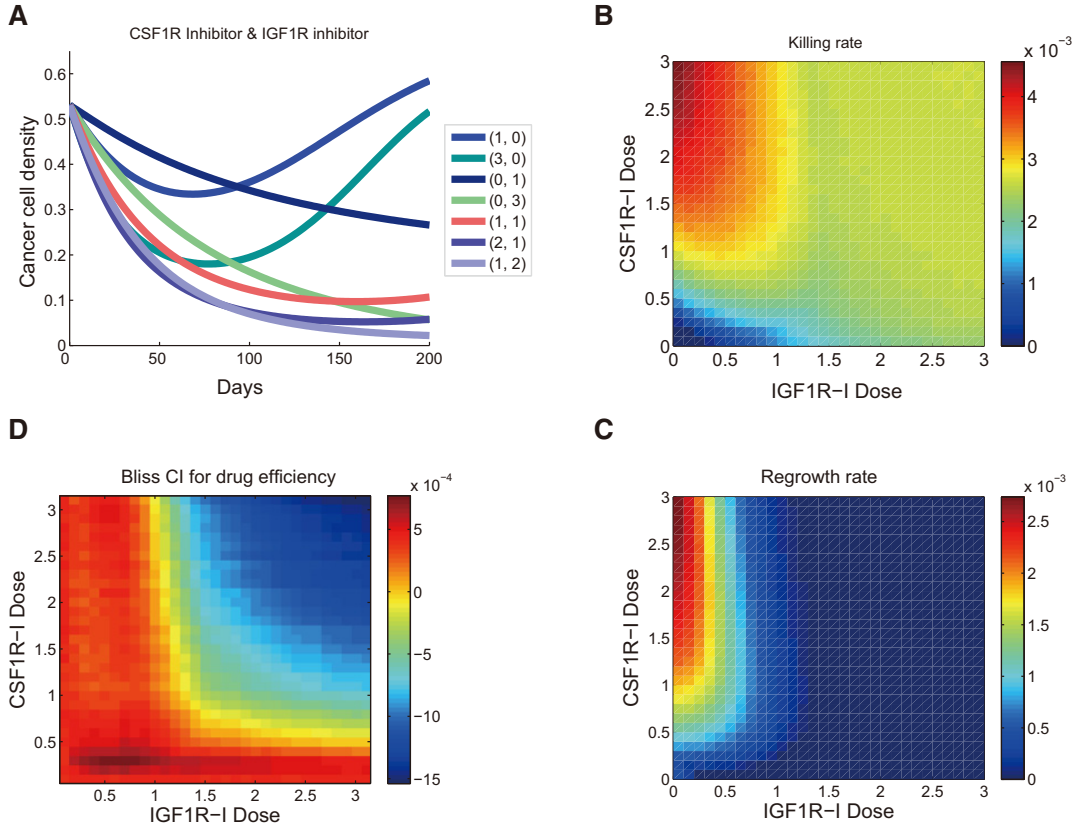

Figure 6.

Evaluation of combination therapy using a CSF1R inhibitor and an IGF1R inhibitor. **A,** Evolution of cancer cell densities with single or combined CSF1R and IGF1R inhibitors. **B,** Dose-dependent killing rate and (**C**) regrowth rate of cancer cells under combined CSF1R inhibition and IGF1R inhibition. **D,** Evaluation of the synergy between CSF1R inhibition and IGF1R inhibition using the Bliss combination index.

that this drug combination exhibited a pattern of dose-dependent synergy and that the synergy decreased as the drug doses increased. This indicates that the efficiency of high drug doses in combination was reduced due to antagonistic effects, although high doses of combined drugs might produce higher killing rates or lower regrowth rates compared with low doses of combined drugs. Considering the increased side effects induced by high doses of drugs, information on how to optimize the doses of combined drugs in combination therapy is very important, especially in the era of precision medicine. In addition, because the killing rate and the regrowth rate of cancer cells have distinct sensitivities to variations in parameters, the timing of the administration of combined drugs might be critical for their long-term treatment effect. Therefore, temporal combinations of multiple drugs with optimized timing and dosing might be more effective than the use of single drugs or simultaneous combinations of drugs (44).

The previous experimental studies have demonstrated that the operations of immune cells and other microenvironmental variables might influence the response of glioma to the treatment (45, 46). As such, besides macrophages modeled in this study, in the future study, we will consider other immune cells that are relevant in gliomas, such as dendritic cells, neutrophils, Treg cells, T effector cells, natural killer cells, etc. (14). In addition, cancer cell populations are heterogeneous and they might react differentially to immune cells. The model could be extended to include cancer stem cells to investigate the heterogeneous response of cancer cells to immunotherapies. Moreover, the *in vivo* data used to estimate the model parameters are indispensable to a more realistic model because the previous relevant works have showed that the slight changes in the model parameter might significantly influence the prediction results (47–49). In future work, we will develop data-driven methods to construct the signaling pathways involved in crosstalk interactions between gliomas and their microenvironments using single cell RNA-seq data and proteomics data. Furthermore, we will build multiscale agent-based models (50) of cell-microenvironment interactions to investigate the intracellular and intercellular mechanisms underlying the drug resistance of cancer cells.

In summary, in this study, we developed a PDE model to quantitatively investigate the mechanisms of interaction between

glioma cells and macrophages that underlie the resistance of these tumor cells to CSF1R inhibition. Our model revealed a dose-dependent resistance mechanism and indicated that a parameter sensitivity switch is triggered by increasing the drug dose. We quantitatively evaluated the synergistic effects of the combination of CSF1R inhibition and IGF1R inhibition. This study advances our understanding of microenvironment-mediated drug resistance and has implications for the design of more effective combination drug therapies to combat drug resistance.

Disclosure of Potential Conflicts of Interest

No potential conflicts of interest were disclosed.

Authors' Contributions

Conception and design: Y. Zheng, X. Sun
Development of methodology: Y. Zheng, X. Sun
Acquisition of data (provided animals, acquired and managed patients, provided facilities, etc.): Y. Zheng
Analysis and interpretation of data (e.g., statistical analysis, biostatistics, computational analysis): Y. Zheng, J. Bao, X. Sun
Writing, review, and/or revision of the manuscript: Y. Zheng, Q. Zhao, T. Zhou, X. Sun
Administrative, technical, or material support (i.e., reporting or organizing data, constructing databases): Y. Zheng, X. Sun
Study supervision: Y. Zheng, X. Sun

Acknowledgments

We would like to acknowledge Dr. Tao Cai at School of Mathematical and Computational Science, Sun Yat-sen University for valuable discussions on numerical simulation. We also thank Prof. Shicheng Su at Sun Yat-Sen Memorial Hospital, Sun Yat-Sen University for help with editing the manuscript. X. Sun was supported by grants from the National Natural Science Foundation of China (61503419), the Guangdong Nature Science Foundation (2014A030310355, 2016A030313234), and the fund for Guangdong Provincial Key Laboratory of Orthopedics and Traumatology (2016B030301002). T. Zhou was supported by grants from the National Key Research Project of China (91530320) and the 973 Project of China (2014CB964703).

The costs of publication of this article were defrayed in part by the payment of page charges. This article must therefore be hereby marked *advertisement* in accordance with 18 U.S.C. Section 1734 solely to indicate this fact.

Received July 6, 2017; revised November 1, 2017; accepted January 18, 2018; published OnlineFirst xx xx, xxxx.

References

1. Junttila MR, de Sauvage FJ. Influence of tumour micro-environment heterogeneity on therapeutic response. Nature 2013;501:346–54.
2. Quail DF, Joyce JA. Microenvironmental regulation of tumor progression and metastasis. Nat Med 2013;19:1423–37.
3. Quail DF, Bowman RL, Akkari L, Quick ML, Schuhmacher AJ, Huse JT, et al. The tumor microenvironment underlies acquired resistance to CSF-1R inhibition in gliomas. Science 2016;352:aad3018.
4. Robert B, Edward C, Luca M, Wilhelm-Benartzi CS, Jane B. Poised epigenetic states and acquired drug resistance in cancer. Nat Rev Cancer 2014;14:747–53.
5. Lee H-J, Zhuang G, Cao Y, Du P, Kim H-J, Settleman J. Drug resistance via feedback activation of Stat3 in oncogene-addicted cancer cells. Cancer Cell 2014;26:207–21.
6. Wagle N, Van Allen EM, Treacy DJ, Frederick DT, Cooper ZA, Taylor-Weiner A, et al. MAP kinase pathway alterations in BRAF-mutant melanoma patients with acquired resistance to combined RAF/MEK inhibition. Cancer Discov 2014;4:61–8.
7. Pazarentzos E, Bivona T. Adaptive stress signaling in targeted cancer therapy resistance. Oncogene 2015;34:5599–606.
8. Dean M, Fojo T, Bates S. Tumour stem cells and drug resistance. Nat Rev Cancer 2005;5:275–84.
9. Cojoc M, Mäbert K, Muders MH, Dubrovska A. A role for cancer stem cells in therapy resistance: cellular and molecular mechanisms. Semin Cancer Biol 2015;31:16–27.
10. Pasipanodya JG, Srivastava S, Gumbo T. Meta-analysis of clinical studies supports the pharmacokinetic variability hypothesis for acquired drug resistance and failure of antituberculosis therapy. Clin Infect Dis 2012;55:169–77.
11. Obenauf AC, Zou Y, Ji AL, Vanharanta S, Shu W, Shi H, et al. Therapy-induced tumour secretomes promote resistance and tumour progression. Nature 2015;520:368.
12. Straussman R, Morikawa T, Shee K, Barzily-Rokni M, Qian ZR, Du J, et al. Tumour micro-environment elicits innate resistance to RAF inhibitors through HGF secretion. Nature 2012;487:500–4.
13. Klemm F, Joyce JA. Microenvironmental regulation of therapeutic response in cancer. Trends Cell Biol 2015;25:198–213.
14. Quail DF, Joyce JA. The microenvironmental landscape of brain tumors. Cancer Cell 2017;31:326.
15. Kerkar SP, Restifo NP. Cellular constituents of immune escape within the tumor microenvironment. Cancer Res 2012;72:3125.
16. Hanahan D, Coussens LM. Accessories to the crime: functions of cells recruited to the tumor microenvironment. Cancer Cell 2012;21:309.
17. Somasundaram R, Zhang G, Fukunaga-Kalabis M, Perego M, Krepler C, Xu X, et al. Tumor-associated B-cells induce tumor heterogeneity and therapy resistance. Nat Commun 2017;8:607.
18. Anderson ARA, Weaver AM, Cummings PT, Quaranta V. Tumor morphology and phenotypic evolution driven by selective pressure from the microenvironment. Cell 2006;127:905–15.
19. Gerlee P, Anderson ARA. An evolutionary hybrid cellular automaton model of solid tumour growth. J Theor Biol 2007;246:583–603.
20. Greaves M, Maley CC. Clonal evolution in cancer. Nature 2012;481:306–13.
21. Merlo LM, Pepper JW, Reid BJ, Maley CC. Cancer as an evolutionary and ecological process. Nat Rev Cancer 2006;6:924–35.
22. Lindsay D, Garvey CM, Mumenthaler SM, Foo J. Leveraging hypoxia-activated prodrugs to prevent drug resistance in solid tumors. PLoS Comput Biol 2016;12:e1005077.
23. Sun X, Bao J, Shao Y. Mathematical modeling of therapy-induced cancer drug resistance: connecting cancer mechanisms to population survival rates. Sci Rep 2016;6:22498.
24. Szomolay B, Eubank TD, Roberts RD, Marsh CB, Friedman A. Modeling the inhibition of breast cancer growth by GM-CSF. J Theor Biol 2012;303:141–51.
25. Knútsdóttir H, Pálsson E, Edelstein-Keshet L. Mathematical model of macrophage-facilitated breast cancer cells invasion. J Theor Biol 2014;357:184–99.
26. Pyonteck SM, Akkari L, Schuhmacher AJ. TAMs are a potential therapeutic target in glioma. Cancer Discov 2013;3:1217.
27. Pyonteck SM, Akkari L, Schuhmacher AJ, Bowman RL, Sevenich L, Quail DF, et al. CSF-1R inhibition alters macrophage polarization and blocks glioma progression. Nat Med 2013;19:1264–72.
28. Gallaher J, Babu A, Plevritis S, Anderson AR. Bridging population and tissue scale tumor dynamics: a new paradigm for understanding differences in tumor growth and metastatic disease. Cancer Res 2014;74:426–35.
29. Wu Y, Lu Y, Chen W, Fu J, Fan R. In silico experimentation of glioma microenvironment development and anti-tumor therapy. PLoS Comput Biol 2012;8:e1002355.
30. Pivonka P, Zimak J, Smith DW, Gardiner BS, Dunstan CR, Sims NA, et al. Model structure and control of bone remodeling: a theoretical study. Bone 2008;43:249–63.
31. Alon U. An introduction to systems biology: design principles of biological circuits. Chapman & Hall/crc Boca Ration Fl 2015;96:15a–a.

32. Sun X, Su J, Bao J, Peng T, Zhang L, Zhang Y, et al. Cytokine combination therapy prediction for bone remodeling in tissue engineering based on the intracellular signaling pathway. Biomaterials 2012;33:8265–76.
33. Lewis CE, Pollard JW. Distinct role of macrophages in different tumor microenvironments. Cancer Res 2006;66:605.
34. Eubank TD, Roberts RD, Khan M, Curry JM, Nuovo GJ, Kuppusamy P, et al. Granulocyte macrophage colony-stimulating factor inhibits breast cancer growth and metastasis by invoking an anti-angiogenic program in tumor-educated macrophages. Cancer Res 2009;69: 2133–40.
35. Chen D, Roda JM, Marsh CB, Eubank TD, Friedman A. Hypoxia inducible factors-mediated inhibition of cancer by GM-CSF: a mathematical model. Bull Math Biol 2012;74:2752–77.
36. De I, Steffen MD, Clark PA, Patros CJ, Sokn E, Bishop SM, et al. CSF1 overexpression promotes high-grade glioma formation without impacting the polarization status of glioma-associated microglia and macrophages. Cancer Res 2016;76:2552.
37. Alterman RL, Stanley ER. Colony stimulating factor-1 expression in human glioma. Mol Chem Neuropathol 1994;21:177.
38. Skeel RD, Berzins M. A method for the spatial discretization of parabolic equations in one space variable. SIAM J. Sci. and Stat. Comput 1987;11:1–32.
39. Marino S, Hogue IB, Ray CJ, Kirschner DE. A methodology for performing global uncertainty and sensitivity analysis in systems biology. J Theor Biol 2008;254:178–96.
40. Bliss C. The toxicity of posons applied jointly. Ann Appl Biol 1939; 26:585–615.
41. Fitzgerald JB, Schoeberl B, Nielsen UB, Sorger PK. Systems biology and combination therapy in the quest for clinical efficacy. Nat Chem Biol 2006;2:458–66.
42. Komohara Y, Ohnishi K, Kuratsu J, Takeya M. Possible involvement of the M2 anti-inflammatory macrophage phenotype in growth of human gliomas. J Pathol 2008;216:15–24.
43. Ruffell B, Coussens LM. Macrophages and therapeutic resistance in cancer. Cancer Cell 2015;27:462–72.
44. Sun X, Hu B. Mathematical modeling and computational prediction of cancer drug resistance. Brief Bioinform 2017. bbx065. Available from: https://doi.org/10.1093/bib/bbx065.
45. Kushchayev SV, Sankar T, Eggink LL, Kushchayeva YS, Wiener PC, Hoober JK, et al. Monocyte galactose/N-acetylgalactosamine-specific C-type lectin receptor stimulant immunotherapy of an experimental glioma. Part 1: stimulatory effects on blood monocytes and monocyte-derived cells of the brain. Cancer Manag Res 2012;4:309.
46. Kushchayev SV, Sankar T, Eggink LL, Kushchayeva YS, Wiener PC, Hoober JK, et al. Monocyte galactose/N-acetylgalactosamine-specific C-type lectin receptor stimulant immunotherapy of an experimental glioma. Part II: combination with external radiation improves survival. Cancer Manag Res 2012;4:325–34.
47. Kostelich EJ, Kuang Y, Mcdaniel JM, Moore NZ, Martirosyan NL, Preul MC. Accurate state estimation from uncertain data and models: an application of data assimilation to mathematical models of human brain tumors. Biol Direct 2011;6:64.
48. Martirosyan NL, Rutter EM, Ramey WL, Kostelich EJ, Kuang Y, Preul MC. Mathematically modeling the biological properties of gliomas: a review. Math Biosci Eng 2015;12:879–905.
49. Rutter EM, Stepien TL, Anderies BJ, Plasencia JD, Woolf EC, Scheck AC, et al. Mathematical analysis of glioma growth in a murine model. Sci Rep 2017;7:2508.
50. Sun X, Kang Y, Bao J, Zhang Y, Yang Y, Zhou X. Modeling vascularized bone regeneration within a porous biodegradable CaP scaffold loaded with growth factors. Biomaterials 2013;34:4971–81.

Supplementary Information

A Spatio-temporal Model of Macrophage-mediated Drug Resistance in Glioma Immunotherapy

Yongjiang Zheng[1], Jiguang Bao[2], Qiyi Zhao[3], Tianshou Zhou[4], Xiaoqiang Sun[5]*

1 Department of Hematology, The Third Affiliated Hospital, Zhong-shan School of Medicine, Sun Yat-Sen University, Guangzhou 510630, China.

2 School of Mathematical Sciences, Beijing Normal University, Beijing 100875, China.

3 Department of Infectious Diseases, Third Affiliated Hospital, Sun Yat-Sen University, Guangzhou 510635, China.

4 School of Mathematical and Computational Science, Sun Yat-Sen University, Guangzhou 510275, China.

5 Zhong-shan School of Medicine, Sun Yat-Sen University, Guangzhou 510080, China; Key Laboratory of Tropical Disease Control (Sun Yat-Sen University), Chinese Ministry of Education, Guangzhou 510080, Guangdong, China.

Corresponding authors:

*Xiaoqiang Sun, Ph.D.

Address: Zhong-shan School of Medicine, Sun Yat-Sen University, Guangzhou 510080, China

E-mail: sunxq6@mail.sysu.edu.cn; xiaoqiangsun88@gmail.com

Text S1. Dimensionless equations.

Text S2. Radial symmetry simplification of the system.

Text S3. Initial and boundary conditions.

Text S4. Parameter estimation.

Text S5. Two-parameter sensitivity analysis.

Text S6. Stochastic simulation and the computation of survival times.

Figure S1. Simulated spatio-temporal profiles of cancer cells and microenvironment using the model with increased drug consumption rate ($10\times\eta_{drug}$).

Figure S2. Model behavior under different values of some critical parameters including r_1, d_1, B_2 and D_d.

Figure S3. Sensitivity analysis for parameter combination.

Figure S4. Dose-dependent sensitivities of the killing rate and the regrowth rate of cancer cells under treatment with different doses of a CSF1R inhibitor.

Figure S5. The dynamics of drug response simulated from the model with initial condition (a) of macrophages as in Text S3.

Figure S6. The dynamics of drug response simulated from the model with initial condition (b) of macrophages as in Text S3.

Table S1. Values of dimensional parameters.

Table S2. Values of dimensionless parameters.

Text S1. Dimensionless equations

To reduce the number of parameters, we simplify the PDE model by rescaling the equations into a dimensionless form. We make the following variable substitutions:

$$x = x^* \cdot \hat{x},\ \ t = t^* \cdot \hat{t},\ \ C_T = C_T{}^* \cdot \hat{C}_T,\ \ C_\phi = C_\phi{}^* \cdot \hat{C}_\phi, [IGF1] = [IGF1]^* \cdot [IGF1]_s,$$
$$[CSF1] = [CSF1]^* \cdot [CSF1]_s, \text{ and } [Drug] = [Drug]^* \cdot [Drug]_s, \tag{S1}$$

where * denotes the dimensional variables.

The scaling parameters are set as follows:

$$\hat{x} = \sqrt{\frac{D_{IGF1}}{d_{IGF1}}},\ \ \hat{t} = \frac{D_{IGF1}}{d_{IGF1} \cdot D_T},\ \ \hat{C}_\phi = C_\phi(x,0) = C_\phi^0,\ \ \hat{C}_T = C_T^{\max},\ \ [CSF1]_s = \frac{S_{CSF1}}{d_{CSF1}} \cdot C_T^{\max},$$
$$[IGF1]_s = \frac{S_{IGF1} \cdot C_\phi^0 \cdot [IL4]_0}{d_{IGF1}}, \text{ and } [Drug]_s = 1. \tag{S2}$$

With the above scaling, the dimensionless equations are obtained as follows:

$$\frac{\partial C_T}{\partial t} = \Delta C_T - A_T \nabla \cdot \left(C_T \nabla [IGF1]\right) + \tilde{\gamma}_T C_T \left(1 - C_T\right) - \tilde{\mu}_T C_T, \tag{S3}$$

$$\frac{\partial C_\phi}{\partial t} = \Delta C_\phi - A_\phi \nabla \cdot \left(C_\phi \nabla [CSF1]\right), \tag{S4}$$

$$\frac{\partial [CSF1]}{\partial t} = \frac{1}{\varepsilon} \Delta [CSF1] + \frac{B_1}{\varepsilon}\left(C_T - [CSF1]\right), \tag{S5}$$

$$\frac{\partial [IGF1]}{\partial t} = \frac{1}{\varepsilon} \Delta [IGF1] + \frac{1}{\varepsilon}\left(C_\phi - [IGF1]\right) + \frac{B_2}{\varepsilon} C_\phi \int_0^t [CSF1R_I](\hat{t} \cdot s) ds, \tag{S6}$$

$$\text{and } \frac{\partial [Drug]}{\partial t} = D_d \Delta [Drug] - \eta_d \cdot C_T. \tag{S7}$$

The new dimensionless parameters are derived from the original parameters as follows:

$$A_T = \frac{a_T}{D_T} \cdot \frac{S_{IGF1} C_\phi^0 [IL4]_0}{d_{IGF1}},\ \ A_\phi = \frac{a_\phi}{D_\phi} \cdot \frac{S_{CSF1} C_T^{max}}{d_{CSF1}}, B_1 = \frac{d_{CSF1}}{d_{IGF1}}, B_2 = \hat{t} \cdot S_{IL4},$$
$$\varepsilon = \frac{D_T}{D_{IGF1}}, D_d = \frac{D_{drug}}{D_T}, \text{ and } \eta_d = \hat{t}\hat{C}_T \eta_{drug} = \frac{1}{\varepsilon} \cdot C_T^{\max} \cdot \frac{\eta_{drug}}{d_{IGF1}}. \tag{S8}$$

Note that ε is a small parameter because the molecular diffusion rate (D_{IGF1}) is much greater than the cell migration velocity (D_T). In addition, the dimensionless regulatory functions of the proliferation and death rates in the above dimensionless equations are as follows:

$$\tilde{\gamma}_T = \frac{D_{IGF1}}{d_{IGF1} \cdot D_T} \cdot r_T \cdot H_1^*(IGF1) \cdot \left(\alpha^* \cdot C_\phi \cdot H_2^*(CSF1R_I)\right), \tag{S9}$$

$$\tilde{\mu}_T = \frac{D_{IGF1}}{d_{IGF1} \cdot D_T} \cdot d_T \cdot \left(1 + \beta^* \cdot C_\phi \cdot H_3^*(CSF1R_I)\right), \tag{S10}$$

where $H_1^*(IGF1) = \dfrac{[IGF1]}{K_1^* + [IGF1]}$, with $K_1^* = K_1 / [IGF1]_s$ and $\alpha^* = \alpha \cdot \hat{C}_\phi$,

$$H_2^*\left(CSF1R_I\right) = \frac{1}{1 + \frac{[CSF1R_I]^*}{K_2}}$$, with $\beta^* = \beta \cdot \hat{C}_\phi$,

and $H_3^*\left(CSF1R_I\right) = \frac{[CSF1R_I]^*}{K_3 + [CSF1R_I]^*}$.

In this way, we reduce the number of key parameters from 15 in the original equations to 9 in the dimensionless model.

Text S2. **Radial symmetry simplification of the system**

For simplicity, we assumed a spherical model for the tumor and its microenvironment. Therefore, the domain we consider is a spheroid. Assuming radial symmetry, the cell density and cytokine concentration evolve in the domain [0, L]. The original model (Eqs. S3-S7) is transformed into the following equations:

$$\frac{\partial C_T}{\partial t} = \frac{1}{r^2}\cdot\frac{\partial}{\partial r}\left(r^2\frac{\partial C_T}{\partial r}\right) - A_T\frac{1}{r^2}\cdot\frac{\partial}{\partial r}\left(r^2 C_T\frac{\partial[IGF1]}{\partial r}\right) + \tilde{\gamma}_T C_T(1-C_T) - \tilde{\mu}_T C_T, \qquad \text{(S11)}$$

$$\frac{\partial C_\phi}{\partial t} = \frac{1}{r^2}\cdot\frac{\partial}{\partial r}\left(r^2\frac{\partial C_\phi}{\partial r}\right) - A_\phi\frac{1}{r^2}\cdot\frac{\partial}{\partial r}\left(r^2 C_\phi\frac{\partial[CSF1]}{\partial r}\right), \qquad \text{(S12)}$$

$$\frac{\partial[CSF1]}{\partial t} = \frac{1}{\varepsilon}\cdot\frac{1}{r^2}\cdot\frac{\partial}{\partial r}\left(r^2\frac{\partial[CSF1]}{\partial r}\right) + \frac{B_1}{\varepsilon}\left(C_T - [CSF1]\right), \qquad \text{(S13)}$$

$$\frac{\partial[IGF1]}{\partial t} = \frac{1}{\varepsilon}\cdot\frac{1}{r^2}\cdot\frac{\partial}{\partial r}\left(r^2\frac{\partial[IGF1]}{\partial r}\right) + \left(C_\phi - [IGF1]\right) + \frac{B_2}{\varepsilon}C_\phi\int_0^t [CSF1R]ds, \qquad \text{(S14)}$$

and $$\frac{\partial[Drug]}{\partial t} = D_d\cdot\frac{1}{r^2}\cdot\frac{\partial}{\partial r}\left(r^2\frac{\partial[Drug]}{\partial r}\right) - \eta_d C_T. \qquad \text{(S15)}$$

Text S3. Initial and boundary conditions

Initial conditions

We assume the following initial conditions:

$$\begin{aligned} &C_T(r,0) = C_0 \times (1+0.1\cdot r_{rand}),\ \ C_\phi(r,0) = 1+0.1\cdot r_{rand}, \\ &[IGF1](r,0) = 1+0.01\cdot r_{rand},\ \ [CSF1](r,0) = f_0\cdot(1+0.01\cdot r_{rand}), \\ &[Drug](r,0) = d_{\max}\cdot r, \end{aligned} \tag{S16}$$

where r_{rand} is a random number subject to the standard normal distribution as in Ref. [1]. For the initial tumor (grade II), $C_0(r,0) = 0.5$, if $r < 0.1\cdot L$; otherwise, $C_0(r,0) = 0$. For high grade tumor, $C_0(r,0) = 0.5$, for all $r \le L$. f_0 is a Heaviside function of $C_T(r,0)$. $d_{\max}$ is the dose of the drug delivered at the boundary of the tumor. Macrophages and IGF1 are assumed to pre-exist in the entire region.

To investigate the effect of spatial distribution of macrophages on the resistance dynamics, we also tested the following initial conditions for macrophages:

(a) $C_\phi(r,0) = (r/L+0.5)+0.1\cdot r_{rand}$;

(b) $C_\phi(r,0) = 2\cdot r/L+0.1\cdot r_{rand}$.

These conditions ensure the equal total density of macrophages. The results were shown in **Fig S3-S4.**

Boundary conditions

At *r*=0, zero flux boundary conditions are imposed for C_T, C_ϕ, [*CSF1*], [*IGF1*] and [*Drug*], and at *r*=*L*, zero flux boundary conditions are imposed for C_T, C_ϕ, [CSF1] and [IGF1], except that $[Drug](L,t) = d_{\max}$. Therefore,

$$\begin{aligned} &\left(\frac{\partial C_T}{\partial r} - A_T C_T \frac{\partial [IGF1]}{\partial r}\right)\Bigg|_{0,\,L} = 0,\ \ \left(\frac{\partial C_\phi}{\partial r} - A_\phi C_T \frac{\partial [CSF1]}{\partial r}\right)\Bigg|_{0,\,L} = 0, \\ &\frac{\partial [CSF1]}{\partial r}\Bigg|_{0,\,L} = 0,\ \ \frac{\partial [IGF1]}{\partial r}\Bigg|_{0,\,L} = 0,\ \ \frac{\partial [Drug]}{\partial r}\Bigg|_{0} = 0,\ \text{and}\ [Drug]\big|_L = d_{\max}. \end{aligned} \tag{S17}$$

Text S4. Parameter estimates

(1) *Diffusion rates*. The diffusion rates of cancer cells and macrophages are assumed to be the same (1.0×10^{-9} cm^2/s [2]), since cancer cells and macrophages move with similar velocities as observed in the experiments [1,3]. The molecular weights of IGF1 and CSF1 are M_1=7649 Da [4] and M_2=60179 Da [1], respectively. The diffusion rates of IGF1 and CSF1 should therefore be scaled by a factor of $\left(M_2/M_1\right)^{1/3}$ $=\left(60179/7649\right)^{1/3}\approx 2$, indicating that these rates are of the same order of magnitude and are therefore assumed to be equal. The diffusion rate of CSF1 has been estimated to be 2×10^{-6} cm^2/s [5-7], which is comparable to the diffusion rate of EGF in rat brain extracellular space ($5.18\times 10^{-7}\sim 16.6\times 10^{-7}$ cm^2/s) measured by integrative optical imaging since they have similar molecular weights [7]. A similar assumption is made for the diffusion rate of the CSF1R inhibitor BLZ945 (molecular weight: 398.48 Da).

(2) *Chemotaxis coefficients*. The chemotaxis coefficient of CSF1 for macrophages is set to be 1.7×10^{-3} cm^2/(s nM), which is taken from the previous works [1,2]. The chemotaxis coefficient of IGF1 for cancer cells is assumed to be the same with that of CSF1 for macrophages, since the tumor cells and macrophages move alongside one another as experiments observed [8,9].

(3) *Growth/death rates*. Based on the results of experimental measurements [10], the basic coefficient of the growth rate of cancer cells is set to 2.41×10^{-5} s^{-1}, a typical value also used in previous works [5,6]. The basic death rate is estimated to be 2.886×10^{-7} s^{-1}, by calibrating the sum of the death rates of cancer cells due to both necrosis and apoptosis [5,6].

(4) *Secretion/degradation rates*. The experimental data [11] indicated that IL4 concentration under the treatment of CSF1R inhibitor for 16 weeks (112 days) is 3.5-fold of that before treatment. Solving Eq. (6), we have

$$[IL4](x,t)=[IL4]_0\cdot\left(1+S_{IL4}\cdot\int_0^t[CSF1R_I](s)ds\right).$$

Setting t=112 in the above equation, we can know $S_{IL4}\cdot\int_0^{112}[CSF1R_I](s)ds$ =2.5 and estimate that the secretion rate of IL4 (S_{IL4}) is 1.2905×10^{-7} s^{-1}. The secretion and degradation rates of CSF1 and IGF1 (3.2×10^{-22} g s^{-1} cell^{-1} and 1.92×10^{-22} g s^{-1} cell^{-1} respectively) are estimated from Refs [5,6], while the degradation rate of the drug is set to be 1×10^{-17} s^{-1} as reported in Ref. [12].

(4) *Other parameters*. Based on the experimental results [13], the maximal carrying capacity of cancer cells ($C_T^{\max}$) and the initial value of the macrophage density (C_ϕ^0) are set to be 1.0×10^9 cells/cm^3 and 2.0×10^8 cells/cm^3, respectively, similar to that in Refs [5,6]. The Michaelis constant of IGF1 in the Hill function of the growth rate (Eq. (S9) in Text S1) is assumed to be comparable to the IGF1 concentration.

Table S1 and **Table S2** list the original parameters and the dimensionless parameters, respectively, used in the simulation. Considering that the values of these parameters may vary over certain ranges, we perform a parameter sensitivity analysis to determine the robustness of the model prediction with such variations; the results suggest that the model is robust with respect to most parameters (see the Results section).

Text S5. Local sensitivity analysis

Single-parameter sensitivity analysis.

A local sensitivity coefficient for the killing rate of cancer cells with respect to parameter p_j is calculated as follows:

$$S_K = \frac{\partial R_K}{\partial p_j} \Big/ \frac{R_K}{p_j} \approx \frac{\Delta R_K}{R_K} \Big/ \frac{\Delta p_j}{p_j}, \text{ for small } \Delta p_j . \tag{S18}$$

Similarly, the sensitivity coefficient for the regrowth rate with respect to parameter p_j was calculated as:

$$S_G = \frac{\partial R_G}{\partial p_j} \Big/ \frac{R_G}{p_j} \approx \frac{\Delta R_G}{R_G} \Big/ \frac{\Delta p_j}{p_j}, \text{ for small } \Delta p_j . \tag{S19}$$

Each parameter is increased by 10% from its estimated value and then the relative changes in the killing arte and regrowth rate as defined by Eq. S18-19 are obtained. Given the randomness of the initial conditions of the model, the computations of the sensitivity coefficients are repeated 20 times, and the mean value and standard deviation are calculated.

Two-parameter sensitivity analysis

To assess the combinatorial effects of the parameters on drug resistance, we perform a two-parameter sensitivity analysis. A local sensitivity coefficient for the killing rate of cancer cells with respect to the parameter pair (p_i, p_j) is calculated as follows:

$$S_K = \frac{\partial^2 R_K}{\partial p_i \partial p_j} \Big/ \frac{R_K}{p_j \cdot p_j} \approx \frac{\Delta R_K}{R_K} \Big/ \left(\frac{\Delta p_i}{p_i} \cdot \frac{\Delta p_j}{p_j} \right), \text{ for small } (\Delta p_i,\ \Delta p_j). \tag{S20}$$

where ΔR_K is the relative change in the killing rate of cancer cells due to a small parameter perturbation $(\Delta p_i,\ \Delta p_j)$.

Similarly, the sensitivity coefficient for the regrowth rate with respect to the parameter p_j is calculated as:

$$S_G = \frac{\partial^2 R_G}{\partial p_i \partial p_j} \Big/ \frac{R_G}{p_j \cdot p_j} \approx \frac{\Delta R_G}{R_G} \Big/ \left(\frac{\Delta p_i}{p_i} \cdot \frac{\Delta p_j}{p_j} \right), \text{ for small } (\Delta p_i,\ \Delta p_j). \tag{S21}$$

The values of each pair of two different parameters are simultaneously altered by 10% from their original values for 4 times (increased or decreased for each parameter in this pair). All other parameters remain at their base values. The relative changes in the killing and regrowth rates, as defined by Eqs. S20-S21, are then obtained. Given the randomness of the initial conditions of the model, the computations of the sensitivity coefficients are repeated 20 times, and the mean value of the results are calculated.

Text S6. **Stochastic simulation and the computation of survival times**

We assumed a bimodal distribution of B_2 and used the Monte Carlo method to simulate the stochastic temporal evolution of cancer cell density in a population of N glioma patients. The bimodal distribution function of B_2 was set to be

$$\rho(x) = \frac{r}{\sigma_1\sqrt{2\pi}}\exp\left(-\frac{(x-\mu_1)^2}{2\sigma_1^{\,2}}\right) + \frac{1-r}{\sigma_1\sqrt{2\pi}}\exp\left(-\frac{(x-\mu_2)^2}{2\sigma_2^{\,2}}\right), \quad x>0, \tag{S22}$$

where $r = 0.6$, $\mu_1 = 2\times B_2$, $\mu_2 = 0.5\times B_2$ and $\sigma_1 = \sigma_2 = 0.5$.

The survival time (T_S) of each patient was calculated as the time period from the initiation of the simulation to the time at which the cell density exceeded a predefined threshold, C_{Th} (assumed to be 0.6 in this work), that is,

$$T_S = \inf\left\{t : C_T(t) \geq C_{Th}\right\}. \tag{S23}$$

Due to the stochastic nature of cancer progression represented by $C_T(t)$, T_S is a random variable. In our simulations, the number of patients, N, was set to 100. We calculated the survival time for each patient, $T_S^{(i)}$, $i = 1, 2, \cdots, N$, according to Eq. (S23). The survival percentage, $SP(t)$, for the entire patient population was computed as

$$SP(t) = card\left(\left\{i : T_S^{(i)} > t\right\}\right)\Big/N, \tag{S24}$$

where $card(A)$ represents the number of elements in set A. The frequency of survival time, $f(t)$, can also be calculated by noting that $SP(t) = 1 - \int_0^t f(s)ds$, or $SP(t_i) = 1 - \sum_{r=0}^{t_i} f(r)$ in the discrete form.

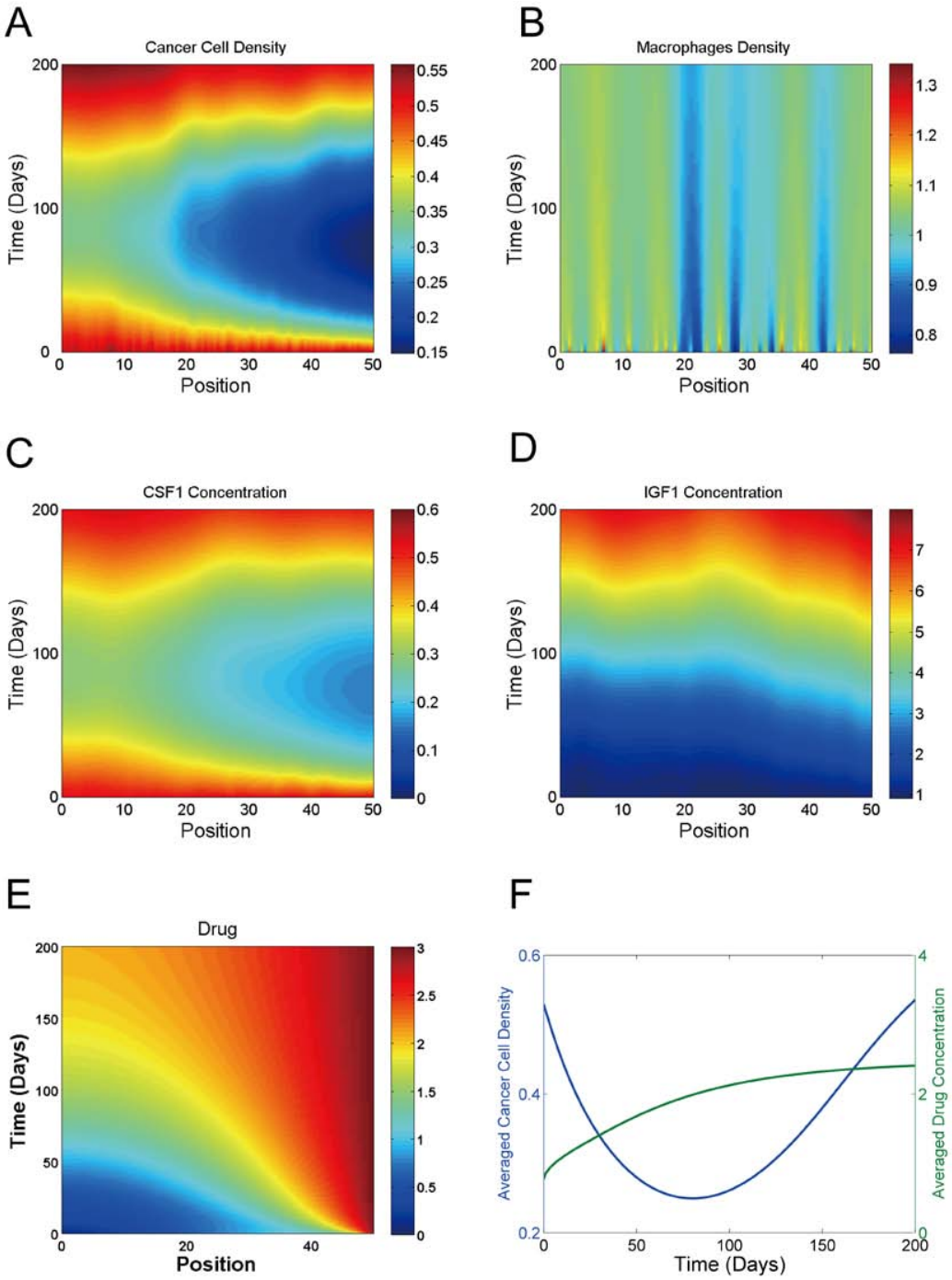

Fig S1. **Simulated spatio-temporal profiles of cancer cells and their microenvironment using the model with increased drug consumption rate** ($10\times\eta_{drug}$). The spatio-temporal distributions of (A) cancer cell density, (B) macrophage density, (C) CSF1 concentration, (D) IGF1 concentration, (E) drug concentration. (F) The time courses of averaged cancer cell density and averaged drug concentration are shown. The simulation showed that increasing drug consumption rate did not significantly influence the emergence of drug resistance (compared to **Fig 2** in the main text).

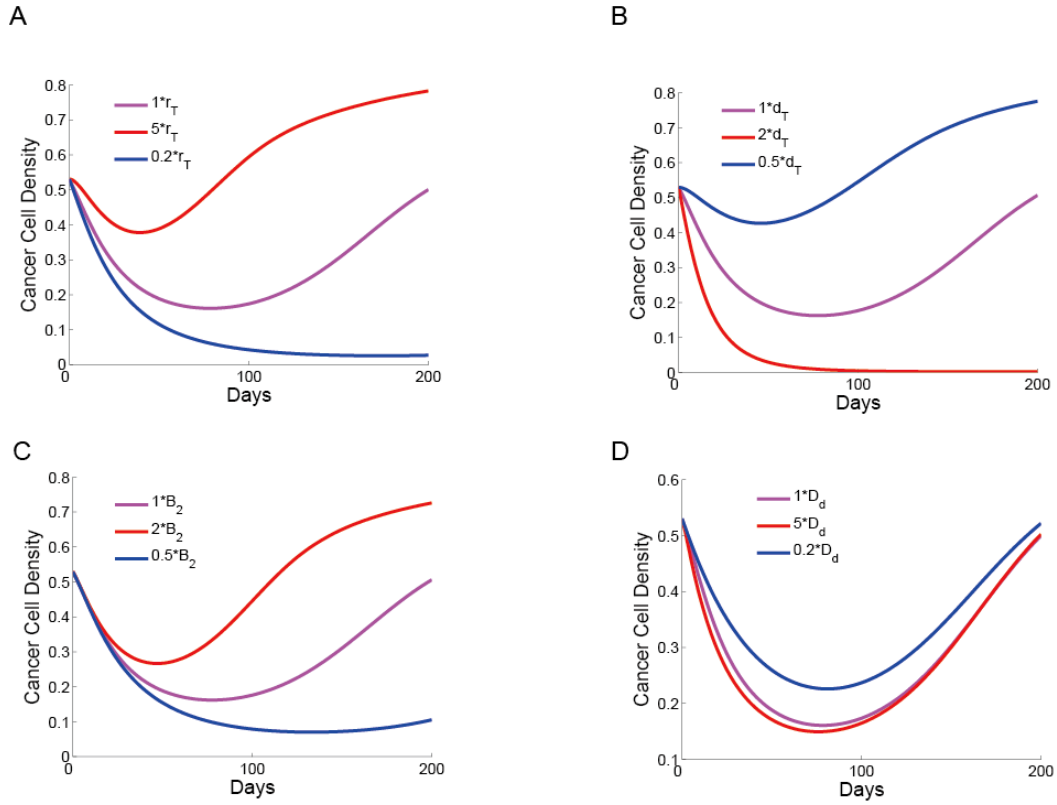

Fig S2. **Model behavior under different values of certain critical parameters, including r_1, d_1, B_2, and D_d.** (A) The decrease in the growth rate of tumor cells, r_1, and (B) the increase of the death rate of tumor cells, d_1, as well as (C) the decrease of the secretion rate of IL4, B_2 , resulted in disappearance of the emergence of drug resistance. (D) The diffusion rate of the drug affected the killing rate and the regrowth rate of cancer cells.

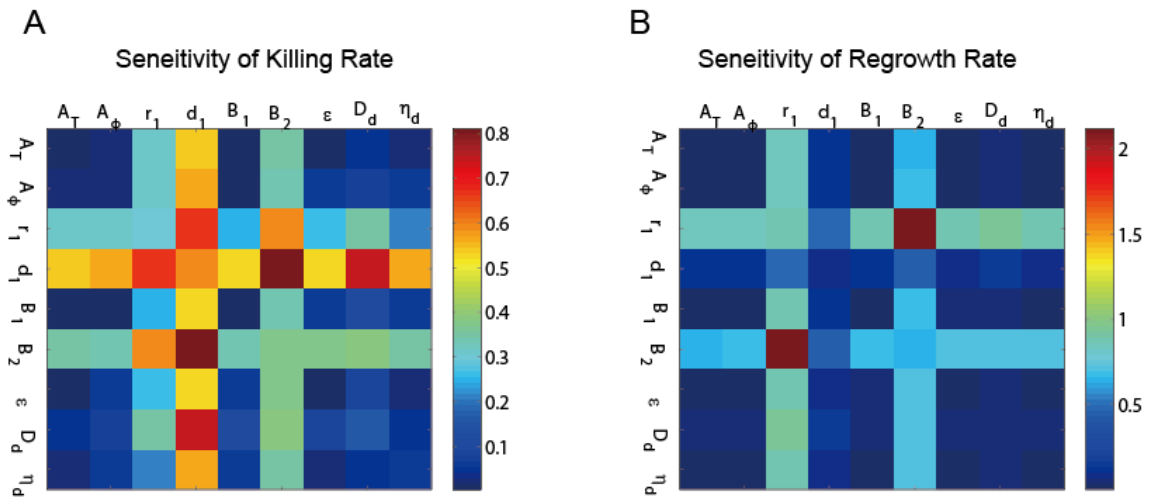

Fig S3. **Sensitivity analysis for parameter combination**. Sensitivity of (A) the cancer cell killing rate and (B) the regrowth rate with respect to combined variations in two parameters. The treatment was conducted with 3 doses of CSF1R inhibitor.

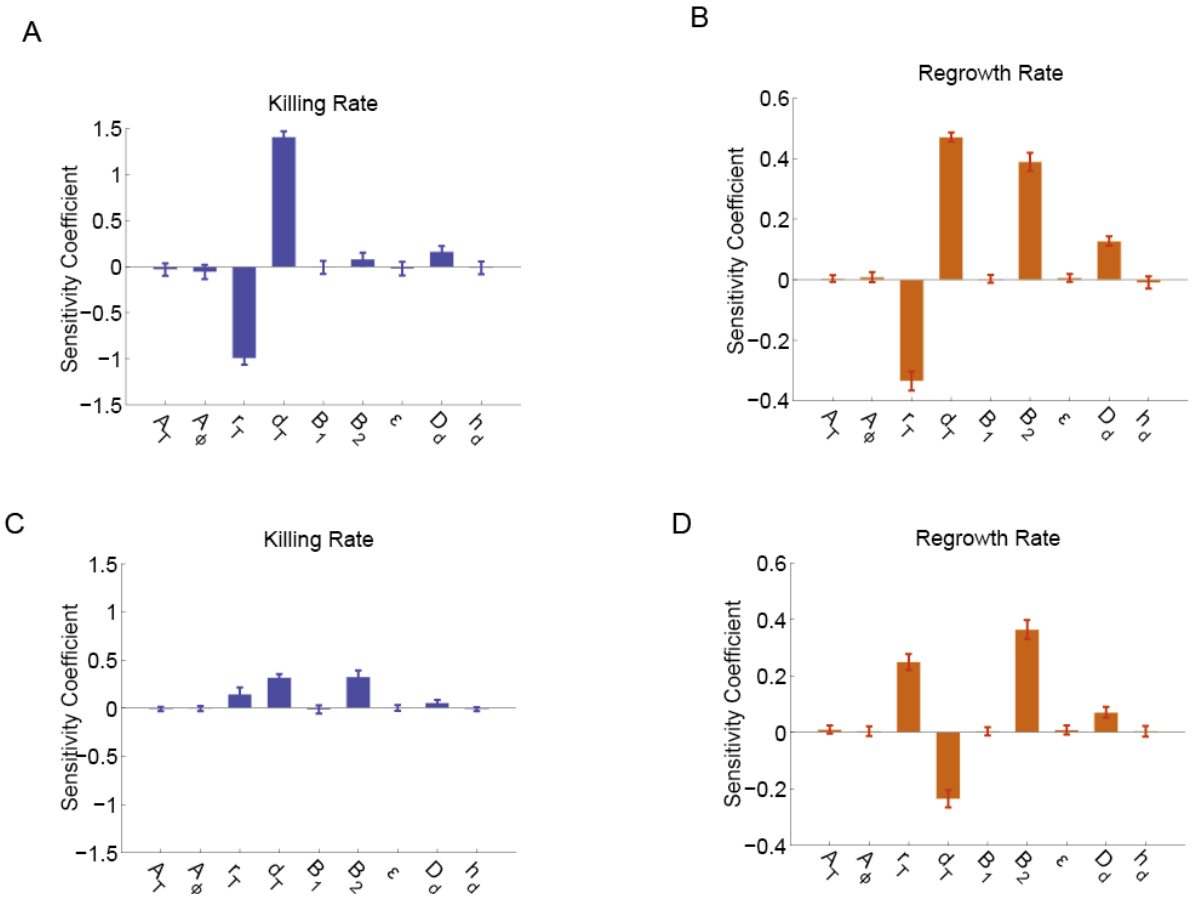

Fig S4. **Dose-dependent sensitivities of the killing rate and the regrowth rate of cancer cells under treatment with different doses of a CSF1R inhibitor [dose 1 (A, B) and dose 3 (C, D)]**. Panels A and B show the sensitivity of the cancer cell killing rate (A) and the regrowth rate (B) to parameter variations during treatment with dose 1 of a CSF1R inhibitor. Panels C and D show the sensitivity of the killing rate (C) and the regrowth rate (D) to parameter variations during treatment with dose 3 of a CSF1R inhibitor.

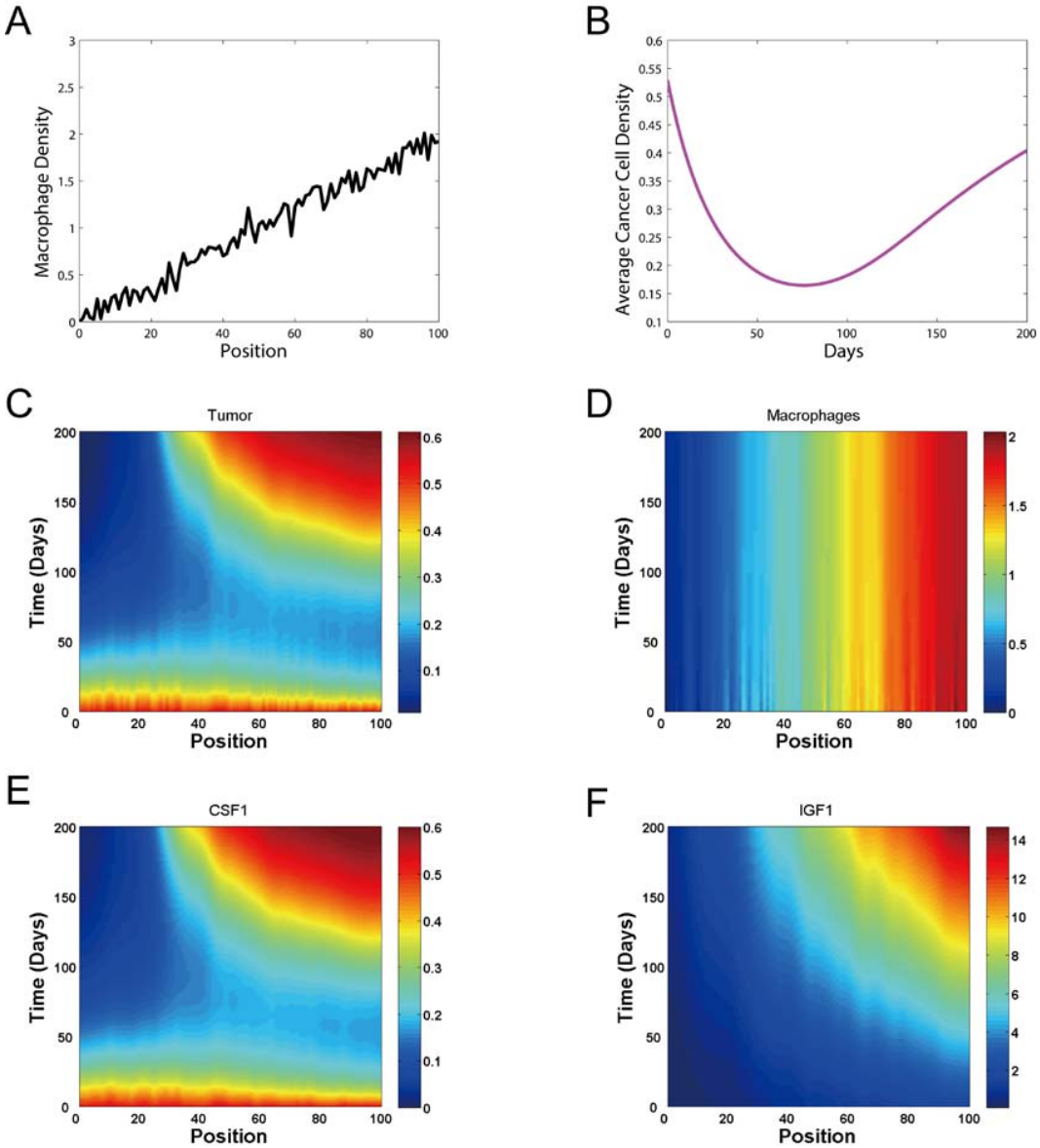

Fig S5. **The dynamics of drug response simulated from the model with initial condition (a) of macrophages as in Text S3**. (A) The initial condition of macrophages. (B) Curves of time course of average cancer cell density. (C-F) The spatio-temporal distributions of cancer cell density (C), macrophage density (D), CSF1 concentration (E), and IGF1 concentration (F).

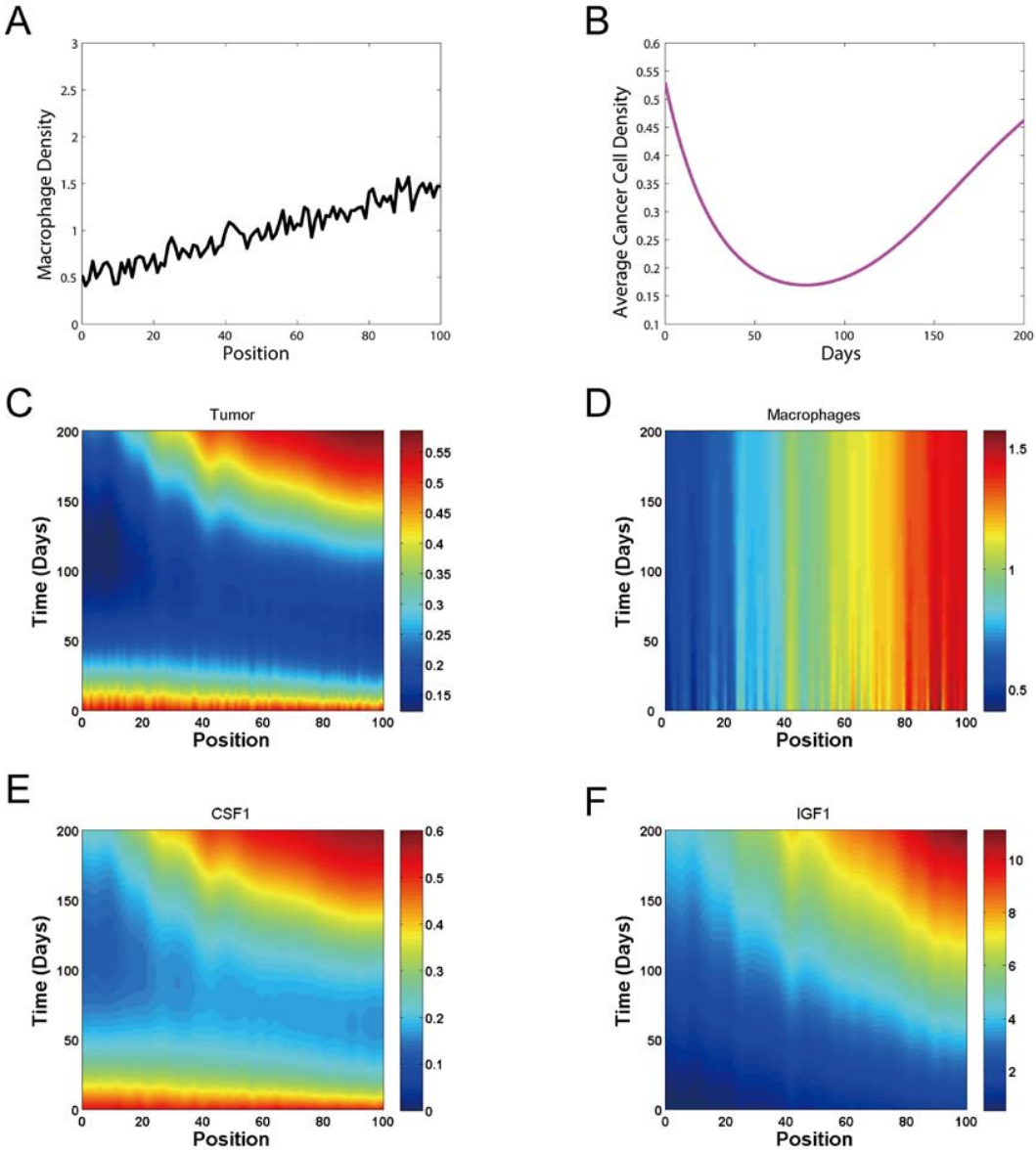

Fig S6. **The dynamics of drug response simulated from the model with initial condition (b) of macrophages as in Text S3**. (A) The initial condition of macrophages. (B) Curves of time course of average cancer cell density. (C-F) The spatio-temporal distributions of cancer cell density (C), macrophage density (D), CSF1 concentration (E), and IGF1 concentratio

Table S1. Values of dimensional parameters. Each parameter is listed with its symbol, value, biological description and reference.

Symbol	Value	Unit	Description	Reference
D_T, D_ϕ	1.0×10^{-9}	cm^2/s	Diffusion coefficient of cancer cells or macrophages	[1,3]
r_T	2.41×10^{-5}	s^{-1}	Growth rate coefficient of cancer cells	[5,6,10]
d_T	2.886×10^{-7}	s^{-1}	Death rate coefficient of cancer cells	[5,6]
a_T, a_ϕ	1.7×10^{-3}	$cm^2/(s\ nM)$	Chemotaxis coefficient of IGF1 (or CSF1) for cancer cells (or macrophages)	[1,2]
D_{CSF1}, D_{IGF1}	2.0×10^{-6}	cm^2/s	Diffusion coefficient of CSF1 or IGF1	[5-7]
S_{CSF1}	3.2×10^{-22}	$g\ s^{-1}\ cell^{-1}$	Secretion rate of CSF1 from cancer cells	[5,6]
S_{IGF1}	1.92×10^{-22}	$g\ s^{-1}\ cell^{-1}$	Secretion rate of IGF1 from cancer cells	[5,6]
d_{CSF1}	5×10^{-4}	s^{-1}	Degradation rate of CSF1	[5,6,14]
d_{IGF1}	2.5×10^{-4}	s^{-1}	Degradation rate of IGF1	[5,6,15]
S_{IL4}	1.2905×10^{-7}	s^{-1}	Secretion rate of IL4	[11]
D_d	2.0×10^{-6}	s^{-1}	Diffusion rate of drug	[5-7]
η_{drug}	1×10^{-17}	s^{-1}	Degradation rate of drug	[12]
K_1	5×10^{-9}	$g\ cm^{-3}$	Michaelis constant of IGF1 in growth rate	Calibrated
α	0.5×10^{-8}	_	a regulatory coefficient corresponding to M2 macrophages' function	Calibrated
β	0.5×10^{-7}	_	a regulatory coefficient corresponding to M1 macrophages' function	Calibrated
$C_T^{\max}$	1.0×10^{9}	$cells\ cm^{-3}$	Maximal carrying capacity of cancer cells	[5,6,13]
C_ϕ^0	2.0×10^{8}	$cells\ cm^{-3}$	Initial value of the density of macrophages	[5,6,13]

Table S2. Values of dimensionless parameters. Each parameter is listed with its symbol, value, biological description and reference.

Symbol	Value	Correspondence to biological meaning
A_T	0.0026	Chemotaxis rate of tumor cells
A_ϕ	0.0109	Chemotaxis rate of macrophages
B_1	2	The ratio of degradation rate of CSF1 to that of IGF1
B_2	1.0324	Secretion rate of IGF1 induced by IL4
ε	5×10^{-4}	Time scale parameter
α	1	A regulatory coefficient for M2 macrophages' function
β	1	A regulatory coefficient for M1 macrophages' function
D_d	2200	Diffusion rate of the drug
η_d	0.08	Degradation/uptake rate of the drug

References

1. Knútsdóttir H, Pálsson E, Edelstein-Keshet L (2014) Mathematical model of macrophage-facilitated breast cancer cells invasion. Journal of Theoretical Biology 357: 184-199.
2. Kim Y, Friedman A (2010) Interaction of Tumor with Its Micro-environment: A Mathematical Model. Bulletin of Mathematical Biology 72: 1029-1068.
3. Goswami S, Sahai E, Wyckoff JB, Cammer M, Cox D, et al. (2005) Macrophages promote the invasion of breast carcinoma cells via a colony-stimulating factor-1/epidermal growth factor paracrine loop. Cancer Research 65: 5278.
4. Rinderknecht E, Humbel RE (1978) The amino acid sequence of human insulin-like growth factor I and its structural homology with proinsulin. Journal of Biological Chemistry 253: 2769-2776.
5. Chen D, Roda JM, Marsh CB, Eubank TD, Friedman A (2012) Hypoxia Inducible Factors-Mediated Inhibition of Cancer by GM-CSF: A Mathematical Model. Bulletin of Mathematical Biology 74: 2752-2777.
6. Szomolay B, Eubank TD, Roberts RD, Marsh CB, Friedman A (2012) Modeling the inhibition of breast cancer growth by GM-CSF. Journal of Theoretical Biology 303: 141-151.
7. Thorne RG, Hrabetová S, Nicholson C (2004) Diffusion of epidermal growth factor in rat brain extracellular space measured by integrative optical imaging. Journal of Neurophysiology 92: 3471-3481.
8. Wyckoff J, Wang W, Lin EY, Wang Y, Pixley F, et al. (2004) A paracrine loop between tumor cells and macrophages is required for tumor cell migration in mammary tumors. Cancer Research 64: 7022.
9. Green CE, Liu T, Montel V, Hsiao G, Lester RD, et al. (2009) Chemoattractant Signaling between Tumor Cells and Macrophages Regulates Cancer Cell Migration, Metastasis and Neovascularization. Plos One 4: e6713.
10. Qian B, Deng Y, Im JH, Muschel RJ, Zou Y, et al. (2009) A distinct macrophage population mediates metastatic breast cancer cell extravasation, establishment and growth. Plos One 4: e6562.
11. Quail DF, Bowman RL, Akkari L, Quick ML, Schuhmacher AJ, et al. (2016) The tumor microenvironment underlies acquired resistance to CSF-1R inhibition in gliomas. Science 352.
12. Frieboes HB, Edgerton ME, Fruehauf JP, Rose FR, Worrall LK, et al. (2009) Prediction of drug response in breast cancer using integrative experimental/computational modeling. Cancer Research 69: 4484-4492.
13. Eubank TD, Roberts RD, Khan M, Curry JM, Nuovo GJ, et al. (2009) Granulocyte macrophage colony-stimulating factor inhibits breast cancer growth and metastasis by invoking an anti-angiogenic program in tumor-educated macrophages. Cancer Research 69: 2133-2140.
14. CM, Pollard JW, Stanley ER (1987) Isolation and characterization of a cloned growth factor dependent macrophage cell line, BAC1.2F5. Journal of Cellular Physiology 130: 420-427.
15. Sorkin A, Duex JE (2010) Quantitative analysis of endocytosis and turnover of epidermal growth factor (EGF) and EGF receptor. Current Protocols in Cell Biology Chapter 15: Unit 15.14.